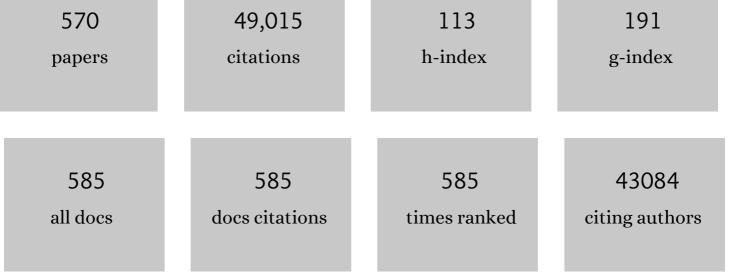
Huijun Zhao

List of Publications by Year in descending order

Source: https://exaly.com/author-pdf/3845580/publications.pdf

Version: 2024-02-01

		1040
570	49,015	113
papers	citations	h-index



2812

#	Article	IF	Citations
1	Ru(bpy)32+-sensitized {001} facets LiCoO2 nanosheets catalyzed CO2 reduction reaction with 100% carbonaceous products. Nano Research, 2022, 15, 1061-1068.	5.8	24
2	Interpolation between W Dopant and Co Vacancy in CoOOH for Enhanced Oxygen Evolution Catalysis. Advanced Materials, 2022, 34, e2104667.	11.1	45
3	Elemental 2D Materials: Solutionâ€Processed Synthesis and Applications in Electrochemical Ammonia Production. Advanced Functional Materials, 2022, 32, 2107280.	7.8	20
4	Molecularly Dispersed Cobalt Phthalocyanine Mediates Selective and Durable CO ₂ Reduction in a Membrane Flow Cell. Advanced Functional Materials, 2022, 32, 2107301.	7.8	43
5	Adsorption and desorption mechanism of aromatic VOCs onto porous carbon adsorbents for emission control and resource recovery: recent progress and challenges. Environmental Science: Nano, 2022, 9, 81-104.	2.2	35
6	hcp-phased Ni nanoparticles with generic catalytic hydrogenation activities toward different functional groups. Science China Materials, 2022, 65, 1252-1261.	3 . 5	5
7	TMN4 complex embedded graphene as efficient and selective electrocatalysts for chlorine evolution reactions. Journal of Electroanalytical Chemistry, 2022, 907, 116071.	1.9	16
8	High-throughput split-protein profiling by combining transposon mutagenesis and regulated protein-protein interactions with deep sequencing. International Journal of Biological Macromolecules, 2022, 203, 543-552.	3.6	0
9	Hollow carbon sphere encapsulated nickel nanoreactor for aqueous-phase hydrogenation-rearrangement tandem reaction with enhanced catalytic performance. Applied Catalysis B: Environmental, 2022, 306, 121140.	10.8	22
10	The stress response mechanisms of biofilm formation under sub-lethal photocatalysis. Applied Catalysis B: Environmental, 2022, 307, 121200.	10.8	24
11	\hat{l}^2 -Arsenene Monolayer: A Promising Electrocatalyst for Anodic Chlorine Evolution Reaction. Catalysts, 2022, 12, 296.	1.6	3
12	Molecularly Dispersed Cobalt Phthalocyanine Mediates Selective and Durable CO ₂ Reduction in a Membrane Flow Cell (Adv. Funct. Mater. 11/2022). Advanced Functional Materials, 2022, 32, .	7.8	1
13	Hydrogen Spillover-Bridged Volmer/Tafel Processes Enabling Ampere-Level Current Density Alkaline Hydrogen Evolution Reaction under Low Overpotential. Journal of the American Chemical Society, 2022, 144, 6028-6039.	6.6	179
14	Enhanced Desalination Performance by a Novel Archimedes Spiral Flow Channel for Flow-Electrode Capacitive Deionization. ACS ES&T Engineering, 2022, 2, 1250-1259.	3.7	15
15	The typical structural evolution of silicon anode. Cell Reports Physical Science, 2022, 3, 100811.	2.8	10
16	Facile synthesis of N, P co-doped carbon encapsulated Ni catalyst for green production of cyclopentanone from biomass derivative furfural. Fuel, 2022, 319, 123815.	3.4	9
17	Low-Dimensional Metal–Organic Frameworks with High Activity and Selectivity toward Electrocatalytic Chlorine Evolution Reactions. Journal of Physical Chemistry C, 2022, 126, 7066-7075.	1.5	20
18	Atomically-dispersed Mn-(N-C2)2(O-C2)2 sites on carbon for efficient oxygen reduction reaction. Energy Storage Materials, 2022, 49, 209-218.	9.5	26

#	Article	lF	Citations
19	Operando Converting BiOCl into Bi2O2(CO3)xCly for Efficient Electrocatalytic Reduction of Carbon Dioxide to Formate. Nano-Micro Letters, 2022, 14, 121.	14.4	15
20	Flow-electrode capacitive deionization utilizing three-dimensional foam current collector for real seawater desalination. Water Research, 2022, 220, 118642.	5.3	27
21	Fabrication of Highâ€Quality CsBi ₃ 1 ₁₀ Films via a Gasâ€Assisted Approach for Efficient Leadâ€Free Perovskite Solar Cells. Energy Technology, 2022, 10, .	1.8	4
22	Synergistic Cr ₂ O ₃ @Ag Heterostructure Enhanced Electrocatalytic CO ₂ Reduction to CO. Advanced Materials, 2022, 34, .	11.1	51
23	Integration of Fe2O3-based photoanode and atomically dispersed cobalt cathode for efficient photoelectrochemical NH3 synthesis. Chinese Chemical Letters, 2021, 32, 805-810.	4.8	13
24	Robust enhanced hydrogen production at acidic conditions over molybdenum oxides-stabilized ultrafine palladium electrocatalysts. Nano Research, 2021, 14, 268-274.	5.8	19
25	Tunable synthesis of imines and secondary-amines from tandem hydrogenation-coupling of aromatic nitro and aldehyde over NiCo5 bi-metallic catalyst. Applied Catalysis B: Environmental, 2021, 280, 119448.	10.8	17
26	Membrane-based colorimetric flow-injection system for online free chlorine monitoring in drinking water. Sensors and Actuators B: Chemical, 2021, 327, 128905.	4.0	10
27	Membrane-Based Portable Colorimetric Gaseous Chlorine Sensing Probe. Analytical Chemistry, 2021, 93, 769-776.	3.2	7
28	Single-atom Fe with Fe1N3 structure showing superior performances for both hydrogenation and transfer hydrogenation of nitrobenzene. Science China Materials, 2021, 64, 642-650.	3.5	98
29	Efficient electrocatalytic nitrogen reduction to ammonia with aqueous silver nanodots. Communications Chemistry, 2021, 4, .	2.0	36
30	Scalable and controllable fabrication of CNTs improved yolk-shelled Si anodes with advanced in operando mechanical quantification. Energy and Environmental Science, 2021, 14, 3502-3509.	15.6	45
31	Converting Co2+-impregnated g-C3N4 into N-doped CNTs-confined Co nanoparticles for efficient hydrogenation rearrangement reactions of furanic aldehydes. Nano Research, 2021, 14, 2846-2852.	5.8	18
32	Synergistic catalysis of cluster and atomic copper induced by copper-silica interface in transfer-hydrogenation. Nano Research, 2021, 14, 4601-4609.	5.8	12
33	Dual-atom Pt heterogeneous catalyst with excellent catalytic performances for the selective hydrogenation and epoxidation. Nature Communications, 2021, 12, 3181.	5.8	156
34	Grey hematite photoanodes decrease the onset potential in photoelectrochemical water oxidation. Science Bulletin, 2021, 66, 1013-1021.	4.3	7
35	Pseudocapacitive desalination via valence engineering with spindle-like manganese oxide/carbon composites. Nano Research, 2021, 14, 4878-4884.	5 . 8	21
36	In Situ Growth of Ultrathin Ni(OH) ₂ Nanosheets as Catalyst for Electrocatalytic Oxidation Reactions. ChemSusChem, 2021, 14, 2935-2942.	3 . 6	35

#	Article	IF	CITATIONS
37	Anchoring Single Copper Atoms to Microporous Carbon Spheres as Highâ€Performance Electrocatalyst for Oxygen Reduction Reaction. Advanced Functional Materials, 2021, 31, 2104864.	7.8	115
38	Intrinsic Pseudocapacitive Affinity in Manganese Spinel Ferrite Nanospheres for High-Performance Selective Capacitive Removal of Ca ²⁺ and Mg ²⁺ . ACS Applied Materials & Interfaces, 2021, 13, 38886-38896.	4.0	20
39	Highly Dispersed Ru Nanoparticles on Boronâ€Doped Ti ₃ C ₂ T <i>_x</i> (MXene) Nanosheets for Synergistic Enhancement of Electrocatalytic Hydrogen Evolution. Small, 2021, 17, e2102218.	5.2	83
40	Crystal plane effect of ceria on supported copper catalyst for liquid-phase hydrogenation of unsaturated aldehyde. Journal of Colloid and Interface Science, 2021, 596, 34-43.	5.0	10
41	Synchronous removal of tetracycline and water hardness ions by capacitive deionization. Journal of Cleaner Production, 2021, 316, 128251.	4.6	17
42	Encapsulated Ni-Co alloy nanoparticles as efficient catalyst for hydrodeoxygenation of biomass derivatives in water. Chinese Journal of Catalysis, 2021, 42, 2027-2037.	6.9	43
43	Metagenomic profiles and health risks of pathogens and antibiotic resistance genes in various industrial wastewaters and the associated receiving surface water. Chemosphere, 2021, 283, 131224.	4.2	39
44	Real-time on-site monitoring of soil ammonia emissions using membrane permeation-based sensing probe. Environmental Pollution, 2021, 289, 117850.	3.7	5
45	Selective electrocatalytic hydrogenation of nitrobenzene over copper-platinum alloying catalysts: Experimental and theoretical studies. Applied Catalysis B: Environmental, 2021, 298, 120545.	10.8	44
46	<i>In situ</i> growth of MOFs on Ni(OH) ₂ for efficient electrocatalytic oxidation of 5-hydroxymethylfurfural. Chemical Communications, 2021, 57, 11358-11361.	2.2	6
47	Rational design of metal oxide catalysts for electrocatalytic water splitting. Nanoscale, 2021, 13, 20324-20353.	2.8	38
48	2D Electrocatalysts for Converting Earthâ€Abundant Simple Molecules into Valueâ€Added Commodity Chemicals: Recent Progress and Perspectives. Advanced Materials, 2020, 32, e1904870.	11.1	76
49	Porous carbon nanosheets functionalized with Fe ₃ O ₄ nanoparticles for capacitive removal of heavy metal ions from water. Environmental Science: Water Research and Technology, 2020, 6, 331-340.	1.2	27
50	CoO _x @Co Nanoparticleâ€based Catalyst for Efficient Selective Transfer Hydrogenation of α,βâ€Unsaturated Aldehydes. ChemCatChem, 2020, 12, 1019-1024.	1.8	10
51	Electrodeposition of hierarchically amorphous FeOOH nanosheets on carbonized bamboo as an efficient filter membrane for As(III) removal. Chemical Engineering Journal, 2020, 392, 123773.	6.6	34
52	Feâ€Co Alloyed Nanoparticles Catalyzing Efficient Hydrogenation of Cinnamaldehyde to Cinnamyl Alcohol in Water. Angewandte Chemie, 2020, 132, 23727-23732.	1.6	1
53	Cobalt-doped Mn3O4 nanocrystals embedded in graphene nanosheets as a high-performance bifunctional oxygen electrocatalyst for rechargeable Zn–Air batteries. Green Energy and Environment, 2020, 5, 499-505.	4.7	59
54	Fast and cost-effective room temperature synthesis of high quality graphene oxide with excellent structural intactness. Sustainable Materials and Technologies, 2020, 25, e00198.	1.7	4

#	Article	IF	Citations
55	Effects of compositional engineering and surface passivation on the properties of halide perovskites: a theoretical understanding. Physical Chemistry Chemical Physics, 2020, 22, 19718-19724.	1.3	11
56	Perovskite Microcrystals with Intercalated Monolayer MoS2 Nanosheets as Advanced Photocatalyst for Solar-Powered Hydrogen Generation. Matter, 2020, 3, 935-949.	5.0	81
57	Selective Growth of Highâ€Density Anatase {101} Twin Boundaries on Highâ€Energy {001} Facets. Small Structures, 2020, 1, 2000025.	6.9	16
58	Coexisting Singleâ€Atomic Fe and Ni Sites on Hierarchically Ordered Porous Carbon as a Highly Efficient ORR Electrocatalyst. Advanced Materials, 2020, 32, e2004670.	11.1	404
59	Rational Design of Cobaltâ€Platinum Alloy Decorated Cobalt Nanoparticles for Oneâ€Pot Synthesis of Imines from Nitroarenes and Aldehydes. ChemCatChem, 2020, 12, 5948-5958.	1.8	10
60	Feâ€Co Alloyed Nanoparticles Catalyzing Efficient Hydrogenation of Cinnamaldehyde to Cinnamyl Alcohol in Water. Angewandte Chemie - International Edition, 2020, 59, 23521-23526.	7.2	91
61	Selective Pseudocapacitive Deionization of Calcium Ions in Copper Hexacyanoferrate. ACS Applied Materials & Samp; Interfaces, 2020, 12, 41437-41445.	4.0	43
62	Materials Science in Australia. Advanced Materials, 2020, 32, e2001629.	11.1	4
63	Electrocatalytically Active Feâ€(Oâ€C ₂) ₄ Singleâ€Atom Sites for Efficient Reduction of Nitrogen to Ammonia. Angewandte Chemie - International Edition, 2020, 59, 13423-13429.	7.2	161
64	Highly dispersed nickel anchored on a N-doped carbon molecular sieve derived from metal–organic frameworks for efficient hydrodeoxygenation in the aqueous phase. Chemical Communications, 2020, 56, 6696-6699.	2.2	17
65	Activation strategies of water-splitting electrocatalysts. Journal of Materials Chemistry A, 2020, 8, 10096-10129.	5.2	67
66	Electrocatalytically Active Feâ€(Oâ€C ₂) ₄ Singleâ€Atom Sites for Efficient Reduction of Nitrogen to Ammonia. Angewandte Chemie, 2020, 132, 13525-13531.	1.6	23
67	Recent Advances in Perovskiteâ€Based Buildingâ€Integrated Photovoltaics. Advanced Materials, 2020, 32, e2000631.	11.1	80
68	Lignosulfonate functionalized g-C ₃ N ₄ /carbonized wood sponge for highly efficient heavy metal ion scavenging. Journal of Materials Chemistry A, 2020, 8, 12687-12698.	5.2	48
69	Hierarchical Co ₃ O ₄ @N-Doped Carbon Composite as an Advanced Anode Material for Ultrastable Potassium Storage. ACS Nano, 2020, 14, 5027-5035.	7.3	121
70	Approaching the activity limit of CoSe2 for oxygen evolution via Fe doping and Co vacancy. Nature Communications, 2020, 11, 1664.	5.8	191
71	Transition Metal (Fe, Co, Mn) Boosting the Lithium Storage of the Multishelled NiO Anode. Energy Technology, 2020, 8, 2000008.	1.8	7
72	Laser Irradiation in Liquid to Release Cobalt Single-Atom Sites for Efficient Electrocatalytic N2 Reduction. ACS Applied Energy Materials, 2020, 3, 6079-6086.	2.5	19

#	Article	IF	Citations
73	How Cobalt and Iron Doping Determine the Oxygen Evolution Electrocatalytic Activity of NiOOH. Cell Reports Physical Science, 2020, 1, 100077.	2.8	35
74	Phosphorus and Sulfur Coâ€Doped Cobaltous Oxide Synthesized by an Inorganicâ€Saltâ€Assisted Method: Reaction Mechanism and Electrocatalytic Application. ChemPlusChem, 2020, 85, 1602-1611.	1.3	4
75	Formation of BNC Coordination to Stabilize the Exposed Active Nitrogen Atoms in $g\hat{a}\in \mathbb{C}$ ₃ N ₄ for Dramatically Enhanced Photocatalytic Ammonia Synthesis Performance. Small, 2020, 16, e1906880.	5.2	88
76	Accelerated evolution of bacterial antibiotic resistance through early emerged stress responses driven by photocatalytic oxidation. Applied Catalysis B: Environmental, 2020, 269, 118829.	10.8	55
77	Fabrication of hierarchically porous NH2-MIL-53/wood-carbon hybrid membrane for highly effective and selective sequestration of Pb2+. Chemical Engineering Journal, 2020, 387, 124141.	6.6	44
78	Ensembles of Photonic Beads: Optical Properties and Enhanced Lightâ€"Matter Interactions. Advanced Optical Materials, 2020, 8, 1901537.	3.6	16
79	Manganese oxides transformed from orthorhombic phase to birnessite with enhanced electrochemical performance as supercapacitor electrodes. Journal of Materials Chemistry A, 2020, 8, 3746-3753.	5.2	22
80	An inverted Bil3/PCBM binary quasi-bulk heterojunction solar cell with a power conversion efficiency of 1.50%. Nano Energy, 2020, 73, 104799.	8.2	17
81	<i>In situ</i> growth of well-aligned Ni-MOF nanosheets on nickel foam for enhanced photocatalytic degradation of typical volatile organic compounds. Nanoscale, 2020, 12, 9462-9470.	2.8	66
82	Stable Seamless Interfaces and Rapid Ionic Conductivity of Ca–CeO ₂ /LiTFSI/PEO Composite Electrolyte for Highâ€Rate and Highâ€Voltage Allâ€Solidâ€State Battery. Advanced Energy Materials, 2020, 10, 2000049.	10.2	252
83	A versatile PDMS submicrobead/graphene oxide nanocomposite ink for the direct ink writing of wearable micron-scale tactile sensors. Applied Materials Today, 2019, 16, 482-492.	2.3	106
84	Recent Progress of Direct Ink Writing of Electronic Components for Advanced Wearable Devices. ACS Applied Electronic Materials, 2019, 1, 1718-1734.	2.0	108
85	The role of electrolyte acid concentration in the electrochemical exfoliation of graphite: Mechanism and synthesis of electrochemical graphene oxide. Nano Materials Science, 2019, 1, 215-223.	3.9	35
86	A Hollowâ€Shell Structured V ₂ O ₅ Electrodeâ€Based Symmetric Full Liâ€Ion Battery with Highest Capacity. Advanced Energy Materials, 2019, 9, 1900909.	10.2	51
87	Liberating Nâ€CNTs Confined Highly Dispersed CoN <i>_x</i> Sites for Selective Hydrogenation of Quinolines. Advanced Materials, 2019, 31, e1906051.	11.1	56
88	Potassiumâ€lonâ€Assisted Regeneration of Active Cyano Groups in Carbon Nitride Nanoribbons: Visibleâ€Lightâ€Driven Photocatalytic Nitrogen Reduction. Angewandte Chemie, 2019, 131, 16797-16803.	1.6	26
89	Potassiumâ€lonâ€Assisted Regeneration of Active Cyano Groups in Carbon Nitride Nanoribbons: Visibleâ€Lightâ€Driven Photocatalytic Nitrogen Reduction. Angewandte Chemie - International Edition, 2019, 58, 16644-16650.	7.2	356
90	Theoretical Understanding of Electrocatalytic Hydrogen Production Performance by Low-Dimensional Metal–Organic Frameworks on the Basis of Resonant Charge-Transfer Mechanisms. Journal of Physical Chemistry Letters, 2019, 10, 6955-6961.	2.1	15

#	Article	IF	CITATIONS
91	Sub-lethal photocatalysis bactericidal technology cause longer persistence of antibiotic-resistance mutant and plasmid through the mechanism of reduced fitness cost. Applied Catalysis B: Environmental, 2019, 245, 698-705.	10.8	24
92	Membrane-based conductivity probe for real-time in-situ monitoring rice field ammonia volatilization. Sensors and Actuators B: Chemical, 2019, 286, 62-68.	4.0	12
93	The electrochemical corrosion of an air thermally-treated carbon fiber cloth electrocatalyst with outstanding oxygen evolution activity under alkaline conditions. Chemical Communications, 2019, 55, 2344-2347.	2.2	10
94	Nitrogenâ€Doped Carbon Nanotube Confined Co–N <i>_×</i> > Sites for Selective Hydrogenation of Biomassâ€Derived Compounds. Advanced Materials, 2019, 31, e1808341.	11.1	138
95	Scalable Production of Graphene Oxide Using a 3D-Printed Packed-Bed Electrochemical Reactor with a Boron-Doped Diamond Electrode. ACS Applied Nano Materials, 2019, 2, 867-878.	2.4	41
96	Experimental and theoretical understanding on electrochemical activation and inactivation processes of Nb ₃ O ₇ (OH) for ambient electrosynthesis of NH ₃ . Journal of Materials Chemistry A, 2019, 7, 16969-16978.	5.2	39
97	Online Conductimetric Flow-Through Analyzer Based on Membrane Diffusion for Ammonia Control in Wastewater Treatment Process. ACS Sensors, 2019, 4, 1881-1888.	4.0	13
98	Encapsulation of Plasmid DNA by Nanoscale Metal–Organic Frameworks for Efficient Gene Transportation and Expression. Advanced Materials, 2019, 31, e1901570.	11.1	130
99	Design of three-dimensional hierarchical TiO ₂ /SrTiO ₃ heterostructures towards selective CO ₂ photoreduction. Inorganic Chemistry Frontiers, 2019, 6, 1667-1674.	3.0	33
100	Enhanced CO ₂ electroreduction performance over Cl-modified metal catalysts. Journal of Materials Chemistry A, 2019, 7, 12420-12425.	5.2	42
101	A hierarchical hybrid monolith: MoS ₄ ^{2â^'} -intercalated NiFe layered double hydroxide nanosheet arrays assembled on carbon foam for highly efficient heavy metal removal. Journal of Materials Chemistry A, 2019, 7, 12869-12881.	5.2	58
102	A Yolk–Shell Structured Silicon Anode with Superior Conductivity and High Tap Density for Full Lithium″on Batteries. Angewandte Chemie - International Edition, 2019, 58, 8824-8828.	7.2	242
103	A Yolk–Shell Structured Silicon Anode with Superior Conductivity and High Tap Density for Full Lithium″on Batteries. Angewandte Chemie, 2019, 131, 8916-8920.	1.6	18
104	Converting eggplant biomass into multifunctional porous carbon electrodes for self-powered capacitive deionization. Environmental Science: Water Research and Technology, 2019, 5, 1054-1063.	1.2	21
105	Regulating the Catalytic Performance of Single-Atomic-Site Ir Catalyst for Biomass Conversion by Metal–Support Interactions. ACS Catalysis, 2019, 9, 5223-5230.	5.5	87
106	Room temperature production of graphene oxide with thermally labile oxygen functional groups forÂimproved lithium ion battery fabrication and performance. Journal of Materials Chemistry A, 2019, 7, 9646-9655.	5.2	27
107	Housing Sulfur in Polymer Composite Frameworks for Li–S Batteries. Nano-Micro Letters, 2019, 11, 17.	14.4	102
108	Catalyst-free activation of persulfate by visible light for water disinfection: Efficiency and mechanisms. Water Research, 2019, 157, 106-118.	5.3	145

#	Article	IF	CITATIONS
109	Construction of Pd/BiOCl Catalyst for Highlyâ€selective Synthesis of Benzoin Ethyl Ether by Chlorine Promoted Coupling Reaction. ChemCatChem, 2019, 11, 2676-2682.	1.8	4
110	Enhancement of the visible-light photocatalytic activity of CeO ₂ by chemisorbed oxygen in the selective oxidation of benzyl alcohol. New Journal of Chemistry, 2019, 43, 7355-7362.	1.4	21
111	Highly sensitive detection of nitrite by using gold nanoparticle-decorated $\hat{l}\pm Fe$ sub>2O ₃ nanorod arrays as self-supporting photo-electrodes. Inorganic Chemistry Frontiers, 2019, 6, 1432-1441.	3.0	18
112	Hierarchical Porous Carbon Materials Derived from Kelp for Superior Capacitive Applications. ACS Sustainable Chemistry and Engineering, 2019, 7, 8735-8743.	3.2	71
113	Ambient Electrosynthesis of Ammonia on a Core–Shellâ€Structured Au@CeO ₂ Catalyst: Contribution of Oxygen Vacancies in CeO ₂ . Chemistry - A European Journal, 2019, 25, 5904-5911.	1.7	69
114	Dramatically Enhanced Ambient Ammonia Electrosynthesis Performance by Inâ€Operando Created Li–S Interactions on MoS ₂ Electrocatalyst. Advanced Energy Materials, 2019, 9, 1803935.	10.2	176
115	Theoretical study of single transition metal atom modified MoP as a nitrogen reduction electrocatalyst. Physical Chemistry Chemical Physics, 2019, 21, 5950-5955.	1.3	43
116	Cu doping in CeO ₂ to form multiple oxygen vacancies for dramatically enhanced ambient N ₂ reduction performance. Chemical Communications, 2019, 55, 2952-2955.	2.2	138
117	EcoMat: Join us in the pursuit of functional materials for green energy and environment. EcoMat, 2019, 1, e12009.	6.8	0
118	Sulfur-doped cobalt oxide nanowires as efficient electrocatalysts for iodine reduction reaction. Journal of Alloys and Compounds, 2019, 772, 80-91.	2.8	11
119	2D–2D Heterostructured UNiMOF/g-C ₃ N ₄ for Enhanced Photocatalytic H ₂ Production under Visible-Light Irradiation. ACS Sustainable Chemistry and Engineering, 2019, 7, 2492-2499.	3.2	90
120	Rapid-Heating-Triggered <i>in Situ</i> Solid-State Transformation of Amorphous TiO ₂ Nanotubes into Well-Defined Anatase Nanocrystals. Crystal Growth and Design, 2019, 19, 1086-1094.	1.4	4
121	Ambient Electrosynthesis of Ammonia on a Biomass-Derived Nitrogen-Doped Porous Carbon Electrocatalyst: Contribution of Pyridinic Nitrogen. ACS Energy Letters, 2019, 4, 377-383.	8.8	142
122	Manipulating the assembled structure of atomically thin CoSe2 nanomaterials for enhanced water oxidation catalysis. Nano Energy, 2019, 57, 371-378.	8.2	23
123	A Gradient Heterostructure Based on Tolerance Factor in Highâ€Performance Perovskite Solar Cells with 0.84 Fill Factor. Advanced Materials, 2019, 31, e1804217.	11.1	95
124	Antibiotic-resistance gene transfer in antibiotic-resistance bacteria under different light irradiation: Implications from oxidative stress and gene expression. Water Research, 2019, 149, 282-291.	5.3	115
125	Wet-chemistry grafted active pyridinic nitrogen sites on holey graphene edges as high performance ORR electrocatalyst for Zn-AirAbatteries. Materials Today Energy, 2019, 11, 24-29.	2.5	23
126	Correlating electrocatalytic activities with sulfur species on sulfur-doped cobalt oxide. Materials Letters, 2019, 236, 614-617.	1.3	2

#	Article	IF	Citations
127	Tungstenâ€Doped Nanocrystalline V ₆ O ₁₃ Nanoparticles as Lowâ€Cost and Highâ€Performance Electrodes for Energy Storage Devices. Energy Technology, 2019, 7, 1801041.	1.8	10
128	Simultaneously high-rate furfural hydrogenation and oxidation upgrading on nanostructured transition metal phosphides through electrocatalytic conversion at ambient conditions. Applied Catalysis B: Environmental, 2019, 244, 899-908.	10.8	115
129	Twoâ€Step Activated Carbon Cloth with Oxygenâ€Rich Functional Groups as a Highâ€Performance Additiveâ€Free Air Electrode for Flexible Zinc–Air Batteries. Advanced Energy Materials, 2019, 9, 1802936.	10.2	170
130	Facile fabrication of composition-tunable Fe/Mg bimetal-organic frameworks for exceptional arsenate removal. Chemical Engineering Journal, 2019, 357, 579-588.	6.6	124
131	Cobalt-based composite films on electrochemically activated carbon cloth as high performance overall water splitting electrodes. International Journal of Hydrogen Energy, 2019, 44, 23-33.	3.8	34
132	Evaluating death and activity decay of Anammox bacteria during anaerobic and aerobic starvation. Chemosphere, 2018, 201, 25-31.	4.2	51
133	Transformation of carbon-encapsulated metallic Co into ultrafine Co/CoO nanoparticles exposed on N-doped graphitic carbon for high-performance rechargeable zinc-air battery. Applied Surface Science, 2018, 448, 369-379.	3.1	31
134	AglnS2/In2S3 heterostructure sensitization of Escherichia coli for sustainable hydrogen production. Nano Energy, 2018, 46, 234-240.	8.2	76
135	Xâ€Shaped αâ€FeOOH with Enhanced Charge Separation for Visibleâ€Lightâ€Driven Photocatalytic Overall Water Splitting. ChemSusChem, 2018, 11, 1365-1373.	3.6	45
136	NiFe-Layered Double Hydroxide Nanosheet Arrays Supported on Carbon Cloth for Highly Sensitive Detection of Nitrite. ACS Applied Materials & Samp; Interfaces, 2018, 10, 6541-6551.	4.0	140
137	Nâ€Modified NiO Surface for Superior Alkaline Hydrogen Evolution. ChemSusChem, 2018, 11, 1020-1024.	3.6	12
138	A Hierarchical Z‑Scheme αâ€Fe ₂ O ₃ /gâ€C ₃ N ₄ Hybrid for Enhanced Photocatalytic CO ₂ Reduction. Advanced Materials, 2018, 30, 1706108.	11.1	761
139	Notable hydrogen production on LaxCa1â^'xCoO3 perovskites via two-step thermochemical water splitting. Journal of Materials Science, 2018, 53, 6796-6806.	1.7	30
140	Enhanced Thermochemical H2 Production on Ca-Doped Lanthanum Manganite Perovskites Through Optimizing the Dopant Level and Re-oxidation Temperature. Acta Metallurgica Sinica (English Letters), 2018, 31, 431-439.	1,5	13
141	Hydroxyapatite nanoparticles in root cells: reducing the mobility and toxicity of Pb in rice. Environmental Science: Nano, 2018, 5, 398-407.	2.2	22
142	Hierarchical MgFe-layered double hydroxide microsphere/graphene composite for simultaneous electrochemical determination of trace Pb(II) and Cd(II). Chemical Engineering Journal, 2018, 347, 953-962.	6.6	86
143	Sulfonate group modified Ni catalyst for highly efficient liquid-phase selective hydrogenation of bio-derived furfural. Chinese Chemical Letters, 2018, 29, 1617-1620.	4.8	22
144	Enhanced Visible-Light-Driven Photocatalytic Bacterial Inactivation by Ultrathin Carbon-Coated Magnetic Cobalt Ferrite Nanoparticles. Environmental Science & Environmental Science & 2018, 52, 4774-4784.	4.6	108

#	Article	IF	CITATIONS
145	Electrolyte Effect on Electrocatalytic Hydrogen Evolution Performance of One-Dimensional Cobalt–Dithiolene Metal–Organic Frameworks: A Theoretical Perspective. ACS Applied Energy Materials, 2018, 1, 1688-1694.	2.5	27
146	Selective Determination of $Cr(VI)$ by Glutaraldehyde Cross-Linked Chitosan Polymer Fluorophores. ACS Sensors, 2018, 3, 792-798.	4.0	60
147	Electrocatalytic oxidation of benzyl alcohol for simultaneously promoting H ₂ evolution by a Co _{0.83} Ni _{0.17} /activated carbon electrocatalyst. New Journal of Chemistry, 2018, 42, 6381-6388.	1.4	27
148	One-step synthesis of cobalt-doped MoS ₂ nanosheets as bifunctional electrocatalysts for overall water splitting under both acidic and alkaline conditions. Chemical Communications, 2018, 54, 3859-3862.	2.2	196
149	Micro/nanostructured porous ZnO as a new DGT binding phase for selective measurement of Cu(II) in water. Colloids and Surfaces A: Physicochemical and Engineering Aspects, 2018, 537, 109-115.	2.3	12
150	Bimetallic Carbide as a Stable Hydrogen Evolution Catalyst in Harsh Acidic Water. ACS Energy Letters, 2018, 3, 78-84.	8.8	42
151	Remarkably enhanced water splitting activity of nickel foam due to simple immersion in a ferric nitrate solution. Nano Research, 2018, 11, 3959-3971.	5.8	88
152	Biomass-derived N-doped porous carbon as electrode materials for Zn-air battery powered capacitive deionization. Chemical Engineering Journal, 2018, 334, 1270-1280.	6.6	182
153	Vapor-phase hydrothermal growth of single crystalline NiS2 nanostructure film on carbon fiber cloth for electrocatalytic oxidation of alcohols to ketones and simultaneous H2 evolution. Nano Research, 2018, 11, 1004-1017.	5.8	56
154	The catalytic behaviour in aqueous-phase hydrogenation over a renewable Ni catalyst derived from a perovskite-type oxide. Dalton Transactions, 2018, 47, 17276-17284.	1.6	9
155	Zirconium metal organic frameworks-based DGT technique for in situ measurement of dissolved reactive phosphorus in waters. Water Research, 2018, 147, 223-232.	5.3	24
156	In Situ Synthesis of Highly Dispersed Cu–Co Bimetallic Nanoparticles for Tandem Hydrogenation/Rearrangement of Bioderived Furfural in Aqueous-Phase. ACS Sustainable Chemistry and Engineering, 2018, 6, 14919-14925.	3.2	46
157	Threeâ€Dimensional Nâ€doped Porous Carbon Derived from Monosodium Glutamate for Capacitive Deionization and the Oxygen Reduction Reaction. ChemElectroChem, 2018, 5, 3873-3880.	1.7	10
158	Correlation between Mechanical Strength of Amorphous TiO ₂ Nanotubes and Their Solid State Crystallization Pathways. ChemistrySelect, 2018, 3, 10711-10716.	0.7	0
159	Ultrathin Nitrogenâ€Doped Holey Carbon@Graphene Bifunctional Electrocatalyst for Oxygen Reduction and Evolution Reactions in Alkaline and Acidic Media. Angewandte Chemie, 2018, 130, 16749-16753.	1.6	49
160	Ultrathin Nitrogenâ€Doped Holey Carbon@Graphene Bifunctional Electrocatalyst for Oxygen Reduction and Evolution Reactions in Alkaline and Acidic Media. Angewandte Chemie - International Edition, 2018, 57, 16511-16515.	7.2	261
161	Highly dispersed Co and Ni nanoparticles encapsulated in N-doped carbon nanotubes as efficient catalysts for the reduction of unsaturated oxygen compounds in aqueous phase. Catalysis Science and Technology, 2018, 8, 5506-5514.	2.1	47
162	Vapor-phase hydrothermal transformation of a nanosheet array structure Ni(OH) ₂ into ultrathin Ni ₃ S ₂ nanosheets on nickel foam for high-efficiency overall water splitting. Journal of Materials Chemistry A, 2018, 6, 19201-19209.	5.2	47

#	Article	IF	Citations
163	Carbothermal Methods: Highly Dispersed Copper Nanoparticles Supported on Activated Carbon as an Efficient Catalyst for Selective Reduction of Vanillin (Small 36/2018). Small, 2018, 14, 1870164.	5. 2	4
164	Nitrogen-free commercial carbon cloth with rich defects for electrocatalytic ammonia synthesis under ambient conditions. Chemical Communications, 2018, 54, 11188-11191.	2.2	79
165	Revealing the Role of Electrocatalyst Crystal Structure on Oxygen Evolution Reaction with Nickel as an Example. Small, 2018, 14, e1802895.	5.2	25
166	Feroxyhyte Nanosheets: Iron Vacancies Induced Bifunctionality in Ultrathin Feroxyhyte Nanosheets for Overall Water Splitting (Adv. Mater. 36/2018). Advanced Materials, 2018, 30, 1870272.	11.1	22
167	Temperature-Controlled Selectivity of Hydrogenation and Hydrodeoxygenation in the Conversion of Biomass Molecule by the Ru ₁ /mpg-C ₃ N ₄ Catalyst. Journal of the American Chemical Society, 2018, 140, 11161-11164.	6.6	199
168	Cobalt Covalent Doping in MoS ₂ to Induce Bifunctionality of Overall Water Splitting. Advanced Materials, 2018, 30, e1801450.	11.1	402
169	Ultrathin Transition Metal Dichalcogenide/3d Metal Hydroxide Hybridized Nanosheets to Enhance Hydrogen Evolution Activity. Advanced Materials, 2018, 30, e1801171.	11.1	180
170	Transfer-hydrogenation of furfural and levulinic acid over supported copper catalyst. Fuel, 2018, 231, 165-171.	3.4	77
171	Enhanced Thermochemical Water Splitting through Formation of Oxygen Vacancy in La _{0.6} Sr _{0.4} BO _{3\hat{a}^3<i>\hat{l}</i>} (B=Cr, Mn, Fe, Co, and Ni) Perovskites. ChemPlusChem, 2018, 83, 924-928.	1.3	19
172	Ball Milling-Induced Plate-like Sub-microstructured Iron for Enhancing Degradation of DDT in a Real Soil Environment. ACS Omega, 2018, 3, 6955-6961.	1.6	5
173	Nature-based catalyst for visible-light-driven photocatalytic CO ₂ reduction. Energy and Environmental Science, 2018, 11, 2382-2389.	15.6	198
174	Few-layer graphdiyne doped with sp-hybridized nitrogen atoms at acetylenic sites for oxygen reduction electrocatalysis. Nature Chemistry, 2018, 10, 924-931.	6.6	558
175	Highly Dispersed Copper Nanoparticles Supported on Activated Carbon as an Efficient Catalyst for Selective Reduction of Vanillin. Small, 2018, 14, e1801953.	5.2	62
176	Iron Vacancies Induced Bifunctionality in Ultrathin Feroxyhyte Nanosheets for Overall Water Splitting. Advanced Materials, 2018, 30, e1803144.	11.1	225
177	Facile synthesis of ultra-thin $CoxNi(1-x)/C$ nano-sheets and their remarkable catalytic properties in 4-nitrophenol reduction. Journal of Environmental Chemical Engineering, 2018, 6, 5239-5248.	3.3	7
178	An efficient and reusable bimetallic Ni3Fe NPs@C catalyst for selective hydrogenation of biomass-derived levulinic acid to \hat{I}^3 -valerolactone. Chinese Journal of Catalysis, 2018, 39, 1599-1607.	6.9	43
179	Spontaneous Redox Approach to the Self-Assembly Synthesis of Au/CeO ₂ Plasmonic Photocatalysts with Rich Oxygen Vacancies for Selective Photocatalytic Conversion of Alcohols. ACS Applied Materials & Diterfaces, 2018, 10, 31394-31403.	4.0	67
180	Sandwich‣ike Reduced Graphene Oxide/Carbon Black/Amorphous Cobalt Borate Nanocomposites as Bifunctional Cathode Electrocatalyst in Rechargeable Zincâ€Air Batteries. Advanced Energy Materials, 2018, 8, 1801495.	10.2	65

#	Article	IF	CITATIONS
181	Engineering Hybrid Guided Modes in Subwavelength Uniaxial Metamaterial Waveguides. Plasmonics, 2017, 12, 245-255.	1.8	1
182	In situ growth of α-Fe ₂ O ₃ nanorod arrays on 3D carbon foam as an efficient binder-free electrode for highly sensitive and specific determination of nitrite. Journal of Materials Chemistry A, 2017, 5, 4726-4736.	5.2	86
183	Activation of persulfates by natural magnetic pyrrhotite for water disinfection: Efficiency, mechanisms, and stability. Water Research, 2017, 112, 236-247.	5.3	176
184	Tropane alkaloids from the Australian plant Triunia montana (Proteaceae). Tetrahedron Letters, 2017, 58, 736-739.	0.7	5
185	Self-assembled Pd/CeO2 catalysts by a facile redox approach for high-efficiency hydrogenation of levulinic acid into gamma-valerolactone. Catalysis Communications, 2017, 93, 10-14.	1.6	37
186	Fewâ€Layer Graphdiyne Nanosheets Applied for Multiplexed Realâ€Time DNA Detection. Advanced Materials, 2017, 29, 1606755.	11.1	198
187	Photocatalytic nanomaterials for solar-driven bacterial inactivation: recent progress and challenges. Environmental Science: Nano, 2017, 4, 782-799.	2.2	239
188	Efficient Synthesis of Furfuryl Alcohol from H ₂ -Hydrogenation/Transfer Hydrogenation of Furfural Using Sulfonate Group Modified Cu Catalyst. ACS Sustainable Chemistry and Engineering, 2017, 5, 2172-2180.	3.2	177
189	Water-soluble inorganic photocatalyst for overall water splitting. Applied Catalysis B: Environmental, 2017, 209, 247-252.	10.8	16
190	Interaction between bacterial cell membranes and nano-TiO2 revealed by two-dimensional FTIR correlation spectroscopy using bacterial ghost as a model cell envelope. Water Research, 2017, 118, 104-113.	5.3	48
191	Two-dimensional CoNi nanoparticles@S,N-doped carbon composites derived from S,N-containing Co/Ni MOFs for high performance supercapacitors. Journal of Materials Chemistry A, 2017, 5, 9873-9881.	5.2	75
192	One-pot redox synthesis of Pt/Fe ₃ O ₄ catalyst for efficiently chemoselective hydrogenation of cinnamaldehyde. RSC Advances, 2017, 7, 21107-21113.	1.7	17
193	Carbon-embedded Ni nanocatalysts derived from MOFs by a sacrificial template method for efficient hydrogenation of furfural to tetrahydrofurfuryl alcohol. Dalton Transactions, 2017, 46, 6358-6365.	1.6	88
194	Low-temperature processed In2S3 electron transport layer for efficient hybrid perovskite solar cells. Nano Energy, 2017, 36, 102-109.	8.2	87
195	Triphasic 2D Materials by Vertically Stacking Laterally Heterostructured 2Hâ€∤1T′â€MoS ₂ on Graphene for Enhanced Photoresponse. Advanced Electronic Materials, 2017, 3, 1700024.	2.6	31
196	Fabrication of Highly Stable Metal Oxide Hollow Nanospheres and Their Catalytic Activity toward 4-Nitrophenol Reduction. ACS Applied Materials & Samp; Interfaces, 2017, 9, 18207-18214.	4.0	97
197	A Bandâ€Edge Potential Gradient Heterostructure to Enhance Electron Extraction Efficiency of the Electron Transport Layer in Highâ€Performance Perovskite Solar Cells. Advanced Functional Materials, 2017, 27, 1700878.	7.8	81
198	Enhanced photocatalytic inactivation of Escherichia coli by a novel Z-scheme g-C 3 N 4 /m-Bi 2 O 4 hybrid photocatalyst under visible light: The role of reactive oxygen species. Applied Catalysis B: Environmental, 2017 , 214 , $23-33$.	10.8	210

#	Article	IF	Citations
199	Carbon-encapsulated heazlewoodite nanoparticles as highly efficient and durable electrocatalysts for oxygen evolution reactions. Nano Research, 2017, 10, 3522-3533.	5.8	27
200	A reliable sewage quality abnormal event monitoring system. Water Research, 2017, 121, 248-257.	5.3	24
201	Earth-abundant Ni2P/g-C3N4 lamellar nanohydrids for enhanced photocatalytic hydrogen evolution and bacterial inactivation under visible light irradiation. Applied Catalysis B: Environmental, 2017, 217, 570-580.	10.8	311
202	î ² -FeOOH Nanorods/Carbon Foam-Based Hierarchically Porous Monolith for Highly Effective Arsenic Removal. ACS Applied Materials & Samp; Interfaces, 2017, 9, 13480-13490.	4.0	143
203	Ca ²⁺ and Ga ³⁺ doped LaMnO ₃ perovskite as a highly efficient and stable catalyst for two-step thermochemical water splitting. Sustainable Energy and Fuels, 2017, 1, 1013-1017.	2.5	37
204	Co ₉ S ₈ @N,P-doped porous carbon electrocatalyst using biomass-derived carbon nanodots as a precursor for overall water splitting in alkaline media. RSC Advances, 2017, 7, 19181-19188.	1.7	69
205	Thermally Induced Crystallization of High Quality CH ₃ NH ₃ PbI ₃ Film with Large Grains for Highly Efficient Perovskite Solar Cells. Chemistry - A European Journal, 2017, 23, 5658-5662.	1.7	6
206	Molten Salt-Assisted Growth of Perovskite Films with Submillimeter-Sized Grains. Industrial & Engineering Chemistry Research, 2017, 56, 524-529.	1.8	3
207	Composite Yttriumâ€Carbonaceous Spheres Templated Multiâ€Shell YVO ₄ Hollow Spheres with Superior Upconversion Photoluminescence. Advanced Materials, 2017, 29, 1604377.	11.1	51
208	S,N-Containing Co-MOF derived Co ₉ S ₈ @S,N-doped carbon materials as efficient oxygen electrocatalysts and supercapacitor electrode materials. Inorganic Chemistry Frontiers, 2017, 4, 491-498.	3.0	108
209	Probing the intracellular organic matters released from the photocatalytic inactivation of bacteria using fractionation procedure and excitation-emission-matrix fluorescence. Water Research, 2017, 110, 270-280.	5. 3	33
210	Highly selective liquid-phase hydrogenation of furfural over N-doped carbon supported metallic nickel catalyst under mild conditions. Molecular Catalysis, 2017, 429, 51-59.	1.0	81
211	Photocatalytic and Photoelectrocatalytic Inactivation Mechanism of Biohazards. Green Chemistry and Sustainable Technology, 2017, , 221-237.	0.4	1
212	Gas-Permeable Membrane-Based Conductivity Probe Capable of In Situ Real-Time Monitoring of Ammonia in Aquatic Environments. Environmental Science & En	4.6	26
213	Bifunctional NH ₂ -MIL-88(Fe) metal–organic framework nanooctahedra for highly sensitive detection and efficient removal of arsenate in aqueous media. Journal of Materials Chemistry A, 2017, 5, 23794-23804.	5.2	230
214	Efficient Synthesis of 2-Methylfuran from Bio-Derived Furfural over Supported Copper Catalyst: The Synergistic Effect of CuO _x and Cu. ChemistrySelect, 2017, 2, 9984-9991.	0.7	14
215	Elimination of antibiotic-resistance bacterium and its associated/dissociative bla and aac(3)-II antibiotic-resistance genes in aqueous system via photoelectrocatalytic process. Water Research, 2017, 125, 219-226.	5.3	67
216	Size Modulation of Zirconium-Based Metal Organic Frameworks for Highly Efficient Phosphate Remediation. ACS Applied Materials & Interfaces, 2017, 9, 32151-32160.	4.0	146

#	Article	IF	Citations
217	Vapour-phase hydrothermal synthesis of Ni2P nanocrystallines on carbon fiber cloth for high-efficiency H2 production and simultaneous urea decomposition. Electrochimica Acta, 2017, 254, 44-49.	2.6	62
218	Rechargeable Batteries: Formation of Septupleâ€Shelled (Co _{2/3} Mn _{1/3} O ₄ Hollow Spheres as Electrode Material for Alkaline Rechargeable Battery (Adv. Mater. 34/2017). Advanced Materials, 2017, 29, .	11.1	12
219	Highly efficient electrocatalytic oxidation of urea on a Mn-incorporated Ni(OH) ₂ /carbon fiber cloth for energy-saving rechargeable Zn–air batteries. Chemical Communications, 2017, 53, 10711-10714.	2.2	32
220	Natural magnetic pyrrhotite as a high-Efficient persulfate activator for micropollutants degradation: Radicals identification and toxicity evaluation. Journal of Hazardous Materials, 2017, 340, 435-444.	6.5	81
221	La1-Ca Mn1-Al O3 perovskites as efficient catalysts for two-step thermochemical water splitting in conjunction with exceptional hydrogen yields. Chinese Journal of Catalysis, 2017, 38, 1079-1086.	6.9	22
222	Formation of Septupleâ€Shelled (Co _{2/3} Mn _{1/3})(Co _{5/6} Mn _{1/6}) ₂ O ₄ Hollow Spheres as Electrode Material for Alkaline Rechargeable Battery. Advanced Materials, 2017, 29, 1700550.	11.1	122
223	Ni ₂ P(O)/Fe ₂ P(O) Interface Can Boost Oxygen Evolution Electrocatalysis. ACS Energy Letters, 2017, 2, 2257-2263.	8.8	173
224	Determination of mercury in aquatic systems by DGT device using thiol-modified carbon nanoparticle suspension as the liquid binding phase. New Journal of Chemistry, 2017, 41, 10305-10311.	1.4	19
225	Renewable Energy Conversion and Storage. Advanced Energy Materials, 2017, 7, 1703091.	10.2	13
226	Palladium-decorated hierarchical titania constructed from the metal-organic frameworks NH2-MIL-125(Ti) as a robust photocatalyst for hydrogen evolution. Applied Catalysis B: Environmental, 2017, 218, 743-750.	10.8	109
227	Genome-scale characterization of RNA tertiary structures and their functional impact by RNA solvent accessibility prediction. Rna, 2017, 23, 14-22.	1.6	28
228	Photoelectrocatalytic Materials for Water Disinfection. Green Chemistry and Sustainable Technology, 2017, , 199-219.	0.4	1
229	Dually Ordered Porous TiO ₂ â€rGO Composites with Controllable Light Absorption Properties for Efficient Solar Energy Conversion. Advanced Materials, 2017, 29, 1604795.	11.1	66
230	Macroscale cobalt-MOFs derived metallic Co nanoparticles embedded in N-doped porous carbon layers as efficient oxygen electrocatalysts. Applied Surface Science, 2017, 392, 402-409.	3.1	92
231	Highly efficient removal of hexavalent chromium in aqueous solutions <i>via</i> chemical reduction of plate-like micro/nanostructured zero valent iron. RSC Advances, 2017, 7, 55905-55911.	1.7	37
232	Chemoselective Transfer Hydrogenation of Cinnamaldehyde over Activated Charcoal Supported Pt/Fe3O4 Catalyst. Chinese Journal of Chemical Physics, 2017, 30, 467-473.	0.6	9
233	A nanoparticulate liquid binding phase based DGT device for aquatic arsenic measurement. Talanta, 2016, 160, 225-232.	2.9	15
234	Oxoacetohydrazideâ€functionalized cellulose with enhanced adsorption performance. Journal of Applied Polymer Science, 2016, 133, .	1.3	7

#	Article	IF	Citations
235	Strongly Coupled CoCr ₂ O ₄ /Carbon Nanosheets as High Performance Electrocatalysts for Oxygen Evolution Reaction. Small, 2016, 12, 2866-2871.	5.2	90
236	Enrichment of SNPs in Functional Categories Reveals Genes Affecting Complex Traits. Human Mutation, 2016, 37, 820-826.	1.1	3
237	Co ₃ O ₄ Hexagonal Platelets with Controllable Facets Enabling Highly Efficient Visible‣ight Photocatalytic Reduction of CO ₂ . Advanced Materials, 2016, 28, 6485-6490.	11.1	395
238	Co/CoO nanoparticles immobilized on Co–N-doped carbon as trifunctional electrocatalysts for oxygen reduction, oxygen evolution and hydrogen evolution reactions. Chemical Communications, 2016, 52, 5946-5949.	2,2	221
239	Controlled growth of CuO/Cu2O hollow microsphere composites as efficient visible-light-active photocatalysts. Applied Catalysis A: General, 2016, 521, 34-41.	2.2	47
240	Fe/Fe2O3 nanoparticles anchored on Fe-N-doped carbon nanosheets as bifunctional oxygen electrocatalysts for rechargeable zinc-air batteries. Nano Research, 2016, 9, 2123-2137.	5.8	116
241	Metal-organic framework derived nitrogen-doped porous carbon@graphene sandwich-like structured composites as bifunctional electrocatalysts for oxygen reduction and evolution reactions. Carbon, 2016, 106, 74-83.	5.4	206
242	Shrimp-shell derived carbon nanodots as precursors to fabricate Fe,N-doped porous graphitic carbon electrocatalysts for efficient oxygen reduction in zinc–air batteries. Inorganic Chemistry Frontiers, 2016, 3, 910-918.	3.0	27
243	Hierarchical iron containing \hat{I}^3 -MnO 2 hollow microspheres: A facile one-step synthesis and effective removal of As(III) via oxidation and adsorption. Chemical Engineering Journal, 2016, 301, 139-148.	6.6	106
244	3D Fe ₃ O ₄ @Au@Ag nanoflowers assembled magnetoplasmonic chains for in situ SERS monitoring of plasmon-assisted catalytic reactions. Journal of Materials Chemistry A, 2016, 4, 8866-8874.	5.2	63
245	Meaningful comparison of photocatalytic properties of {001} and {101} faceted anatase TiO2 nanocrystals. Science Bulletin, 2016, 61, 1003-1012.	4.3	30
246	TiO ₂ cement for high-performance dye-sensitized solar cells. RSC Advances, 2016, 6, 83802-83807.	1.7	3
247	Co/Co9S8@S,N-doped porous graphene sheets derived from S, N dual organic ligands assembled Co-MOFs as superior electrocatalysts for full water splitting in alkaline media. Nano Energy, 2016, 30, 93-102.	8.2	260
248	Metal–organic frameworks as selectivity regulators for hydrogenation reactions. Nature, 2016, 539, 76-80.	13.7	1,201
249	Ultrafine nickel–cobalt alloy nanoparticles incorporated into three-dimensional porous graphitic carbon as an electrode material for supercapacitors. Journal of Materials Chemistry A, 2016, 4, 17080-17086.	5.2	53
250	Synthesis of multi-shelled MnO ₂ hollow microspheres via an anion-adsorption process of hydrothermal intensification. Inorganic Chemistry Frontiers, 2016, 3, 1065-1070.	3.0	60
251	Fabrication of hierarchical iron-containing MnO ₂ hollow microspheres assembled by thickness-tunable nanosheets for efficient phosphate removal. Journal of Materials Chemistry A, 2016, 4, 14814-14826.	5.2	60
252	Ultrathin metalâ€"organic framework nanosheets for electrocatalytic oxygen evolution. Nature Energy, 2016, 1, .	19.8	1,979

#	Article	IF	Citations
253	Functionalization of perovskite thin films with moisture-tolerant molecules. Nature Energy, 2016, 1, .	19.8	439
254	Multi-shelled metal oxides prepared via an anion-adsorption mechanism for lithium-ion batteries. Nature Energy, 2016, 1, .	19.8	352
255	One-step solid phase synthesis of a highly efficient and robust cobalt pentlandite electrocatalyst for the oxygen evolution reaction. Journal of Materials Chemistry A, 2016, 4, 18314-18321.	5.2	97
256	Differences in photoelectrocatalytic inactivation processes between E. coli and its isogenic single gene knockoff mutants: Destruction of membrane framework or associated proteins?. Applied Catalysis B: Environmental, 2016, 188, 360-366.	10.8	34
257	Enhanced simultaneous PEC eradication of bacteria and antibiotics by facilely fabricated high-activity {001} facets TiO2 mounted onto TiO2 nanotubular photoanode. Water Research, 2016, 101, 597-605.	5.3	46
258	Molecular engineering of Ni–/Co–porphyrin multilayers on reduced graphene oxide sheets as bifunctional catalysts for oxygen evolution and oxygen reduction reactions. Chemical Science, 2016, 7, 5640-5646.	3.7	120
259	Synergistic photocatalytic inactivation mechanisms of bacteria by graphene sheets grafted plasmonic Ag AgX (XÂ=ÂCl, Br, I) composite photocatalyst under visible light irradiation. Water Research, 2016, 99, 149-161.	5.3	122
260	Fluorescence Determination of Nitrite in Water Using Prawn-Shell Derived Nitrogen-Doped Carbon Nanodots as Fluorophores. ACS Sensors, 2016, 1, 875-881.	4.0	126
261	Soft-template assisted synthesis of mesoporous CuO/Cu 2 O composite hollow microspheres as efficient visible-light photocatalyst. Materials Letters, 2016, 182, 47-51.	1.3	26
262	The surface sulfur doping induced enhanced performance of cobalt catalysts in oxygen evolution reactions. Chemical Communications, 2016, 52, 9450-9453.	2.2	47
263	Growth and in situ transformation of TiO2 and HTiOF3 crystals on chitosan-polyvinyl alcohol co-polymer substrates under vapor phase hydrothermal conditions. Nano Research, 2016, 9, 745-754.	5.8	19
264	The role of catalase and H2O2 in photocatalytic inactivation of Escherichia coli: Genetic and biochemical approaches. Catalysis Today, 2016, 266, 205-211.	2.2	9
265	Shrimp-shell derived carbon nanodots as carbon and nitrogen sources to fabricate three-dimensional N-doped porous carbon electrocatalysts for the oxygen reduction reaction. Physical Chemistry Chemical Physics, 2016, 18, 4095-4101.	1.3	97
266	Unveiling the photoelectrocatalytic inactivation mechanism of Escherichia coli: Convincing evidence from responses of parent and anti-oxidation single gene knockout mutants. Water Research, 2016, 88, 135-143.	5. 3	50
267	Boron doped BiOBr nanosheets with enhanced photocatalytic inactivation of Escherichia coli. Applied Catalysis B: Environmental, 2016, 192, 35-45.	10.8	213
268	Photocatalytic inactivation of Escherichia coli—The roles of genes in β-oxidation of fatty acid degradation. Catalysis Today, 2016, 266, 219-225.	2.2	6
269	Hollow mesoporous SiO ₂ sphere nanoarchitectures with encapsulated silver nanoparticles for catalytic reduction of 4-nitrophenol. Inorganic Chemistry Frontiers, 2016, 3, 663-670.	3.0	27
270	Numerical Modelling of Pore Pressure Accumulations in Marine Sediments around Submerged Breakwaters under Combined Wave and Current Loadings. Journal of Coastal Research, 2016, 321, 1092-1104.	0.1	3

#	Article	IF	Citations
271	Enhanced removal of trace Cr(VI) from neutral and alkaline aqueous solution by FeCo bimetallic nanoparticles. Journal of Colloid and Interface Science, 2016, 472, 8-15.	5.0	51
272	A novel method developed for estimating mineralization efficiencies and its application in PC and PEC degradations of large molecule biological compounds with unknown chemical formula. Water Research, 2016, 95, 150-158.	5.3	9
273	Engineered Hematite Mesoporous Single Crystals Drive Drastic Enhancement in Solar Water Splitting. Nano Letters, 2016, 16, 427-433.	4.5	80
274	The influence of biochar type on long-term stabilization for Cd and Cu in contaminated paddy soils. Journal of Hazardous Materials, 2016, 304, 40-48.	6.5	195
275	3D graphene/Î-MnO ₂ aerogels for highly efficient and reversible removal of heavy metal ions. Journal of Materials Chemistry A, 2016, 4, 1970-1979.	5.2	257
276	Highly Ordered Single Crystalline Nanowire Array Assembled Three-Dimensional Nb ₃ O ₇ (OH) and Nb ₂ O ₅ Superstructures for Energy Storage and Conversion Applications. ACS Nano, 2016, 10, 507-514.	7.3	81
277	Controllable synthesis of mesostructures from TiO ₂ hollow to porous nanospheres with superior rate performance for lithium ion batteries. Chemical Science, 2016, 7, 793-798.	3.7	147
278	Electrodes: A New Graphdiyne Nanosheet/Pt Nanoparticle-Based Counter Electrode Material with Enhanced Catalytic Activity for Dye-Sensitized Solar Cells (Adv. Energy Mater. 12/2015). Advanced Energy Materials, 2015, 5, n/a-n/a.	10.2	1
279	Switching the photocatalytic activity of g-C3N4 by homogenous surface chemical modification with nitrogen residues and vacancies. RSC Advances, 2015, 5, 21430-21433.	1.7	21
280	Adsorption of Hg ²⁺ by thiol functionalized hollow mesoporous silica microspheres with magnetic cores. RSC Advances, 2015, 5, 51446-51453.	1.7	45
281	Enhanced visible-light-driven photocatalytic inactivation of Escherichia coli using g-C3N4/TiO2 hybrid photocatalyst synthesized using a hydrothermal-calcination approach. Water Research, 2015, 86, 17-24.	5.3	323
282	Extending the photoelectrocatalytic detection range of KHP by eliminating self-inhibition at TiO2 nanoparticle electrodes. Journal of Electroanalytical Chemistry, 2015, 738, 209-216.	1.9	8
283	Adsorption and oxidation of oxalic acid on anatase TiO2 (001) surface: A density functional theory study. Journal of Colloid and Interface Science, 2015, 454, 180-186.	5.0	22
284	Dual Roles of Capsular Extracellular Polymeric Substances in Photocatalytic Inactivation of Escherichia coli: Comparison of E. coli BW25113 and Isogenic Mutants. Applied and Environmental Microbiology, 2015, 81, 5174-5183.	1.4	37
285	The search for efficient electrocatalysts as counter electrode materials for dye-sensitized solar cells: mechanistic study, material screening and experimental validation. NPG Asia Materials, 2015, 7, e226-e226.	3.8	52
286	Improved conductivity of NdFeO ₃ through partial substitution of Nd by Ca: a theoretical study. Physical Chemistry Chemical Physics, 2015, 17, 29097-29102.	1.3	9
287	Poro-Elasto-Plastic Model for the Wave-Induced Liquefaction 1. Journal of Offshore Mechanics and Arctic Engineering, 2015, 137, .	0.6	33
288	Dual-functional gum arabic binder for silicon anodes in lithium ion batteries. Nano Energy, 2015, 12, 178-185.	8.2	236

#	Article	IF	Citations
289	Low cost and environmentally benign crack-blocking structures for long life and high power Si electrodes in lithium ion batteries. Journal of Materials Chemistry A, 2015, 3, 2036-2042.	5.2	53
290	Role of <i>in Situ</i> Resultant H ₂ O ₂ in the Visible-Light-Driven Photocatalytic Inactivation of <i>E. coli</i> Using Natural Sphalerite: A Genetic Study. Journal of Physical Chemistry B, 2015, 119, 3104-3111.	1.2	29
291	Photoelectrochemical determination of intrinsic kinetics of photoelectrocatalysis processes at {001} faceted anatase TiO ₂ photoanodes. RSC Advances, 2015, 5, 12860-12865.	1.7	17
292	Cross-linked ZnIn 2 S 4 /rGO composite photocatalyst for sunlight-driven photocatalytic degradation of 4-nitrophenol. Applied Catalysis B: Environmental, 2015, 168-169, 266-273.	10.8	101
293	Surface capacitive contributions: Towards high rate anode materials for sodium ion batteries. Nano Energy, 2015, 12, 224-230.	8.2	371
294	One pot microwave-assisted synthesis of Ag decorated yolk@shell structured TiO2 microspheres. RSC Advances, 2015, 5, 11349-11357.	1.7	5
295	An in situ vapour phase hydrothermal surface doping approach for fabrication of high performance Co ₃ O ₄ electrocatalysts with an exceptionally high S-doped active surface. Chemical Communications, 2015, 51, 5695-5697.	2.2	47
296	Modified natural diatomite and its enhanced immobilization of lead, copper and cadmium in simulated contaminated soils. Journal of Hazardous Materials, 2015, 289, 210-218.	6.5	80
297	Ultrathin platinum nanowires grown on single-layered nickel hydroxide with high hydrogen evolution activity. Nature Communications, 2015, 6, 6430.	5.8	848
298	Nitrogen-Doped Carbon Nanodots@Nanospheres as An Efficient Electrocatalyst for Oxygen Reduction Reaction. Electrochimica Acta, 2015, 165, 7-13.	2.6	41
299	Micro/nanostructured porous Fe–Ni binary oxide and its enhanced arsenic adsorption performances. Journal of Colloid and Interface Science, 2015, 458, 94-102.	5.0	45
300	Rutile {111} Faceted TiO ₂ Film with High Ability for Selective Adsorption of Aldehyde. Journal of Physical Chemistry C, 2015, 119, 17680-17686.	1.5	7
301	Visible-light-driven inactivation of Escherichia coli K-12 over thermal treated natural pyrrhotite. Applied Catalysis B: Environmental, 2015, 176-177, 749-756.	10.8	50
302	Photoelectrochemical manifestation of intrinsic photoelectron transport properties of vertically aligned {001} faceted single crystal TiO ₂ nanosheet films. RSC Advances, 2015, 5, 55438-55444.	1.7	15
303	Hyper-Branched Cu@Cu ₂ O Coaxial Nanowires Mesh Electrode for Ultra-Sensitive Glucose Detection ACS Applied Materials & Samp; Interfaces, 2015, 7, 16802-16812.	4.0	99
304	Epitaxial growth of hyperbranched Cu/Cu2O/CuO core-shell nanowire heterostructures for lithium-ion batteries. Nano Research, 2015, 8, 2763-2776.	5.8	68
305	Enhancement of zinc vacancies in room-temperature ferromagnetic Cr–Mn codoped ZnO nanorods synthesized by hydrothermal method under high pulsed magnetic field. Journal of Alloys and Compounds, 2015, 647, 823-829.	2.8	21
306	Multi-shelled hollow micro-/nanostructures. Chemical Society Reviews, 2015, 44, 6749-6773.	18.7	603

#	Article	IF	Citations
307	Photocatalytic and photoelectrocatalytic degradation and mineralization of small biological compounds amino acids at TiO2 photoanodes. Catalysis Today, 2015, 245, 46-53.	2.2	13
308	A fluorescent quenching performance enhancing principle for carbon nanodot-sensitized aqueous solar cells. Nano Energy, 2015, 13, 124-130.	8.2	34
309	Thiourea sole doping reagent approach for controllable N, S co-doping of pre-synthesized large-sized carbon nanospheres as electrocatalyst for oxygen reduction reaction. Carbon, 2015, 92, 339-347.	5 . 4	59
310	Carbon for the oxygen reduction reaction: a defect mechanism. Journal of Materials Chemistry A, 2015, 3, 11736-11739.	5.2	261
311	A New Graphdiyne Nanosheet/Pt Nanoparticleâ€Based Counter Electrode Material with Enhanced Catalytic Activity for Dyeâ€Sensitized Solar Cells. Advanced Energy Materials, 2015, 5, 1500296.	10.2	180
312	The role and synergistic effect of the light irradiation and H2O2 in photocatalytic inactivation of Escherichia coli. Journal of Photochemistry and Photobiology B: Biology, 2015, 149, 164-171.	1.7	22
313	Mechanistic study of the visible-light-driven photocatalytic inactivation of bacteria by graphene oxide–zinc oxide composite. Applied Surface Science, 2015, 358, 137-145.	3.1	48
314	A fluorescent chitosan hydrogel detection platform for the sensitive and selective determination of trace mercury(<scp>ii</scp>) in water. Journal of Materials Chemistry A, 2015, 3, 19455-19460.	5.2	66
315	Micro/nano-scaled carbon spheres based on hydrothermal carbonization of agarose. Colloids and Surfaces A: Physicochemical and Engineering Aspects, 2015, 484, 386-393.	2.3	53
316	Local atomic structure modulations activate metal oxide as electrocatalyst for hydrogen evolution in acidic water. Nature Communications, 2015, 6, 8064.	5.8	270
317	A low-cost cementite (Fe ₃ C) nanocrystal@N-doped graphitic carbon electrocatalyst for efficient oxygen reduction. Physical Chemistry Chemical Physics, 2015, 17, 27527-27533.	1.3	22
318	Growth of Polypyrrole Ultrathin Films on MoS ₂ Monolayers as Highâ€Performance Supercapacitor Electrodes. Advanced Materials, 2015, 27, 1117-1123.	11.1	691
319	A photochromic naphthopyran dye activated by the intramolecular hydrogen bond and its photodynamics in the ormosil matrix coating. Journal of Sol-Gel Science and Technology, 2015, 73, 293-298.	1.1	13
320	Density Functional Studies of Stoichiometric Surfaces of Orthorhombic Hybrid Perovskite CH ₃ NH ₃ Pbl ₃ . Journal of Physical Chemistry C, 2015, 119, 1136-1145.	1.5	73
321	Self-supported bimodal-pore structured nitrogen-doped carbon fiber aerogel as electrocatalyst for oxygen reduction reaction. Electrochemistry Communications, 2015, 51, 6-10.	2.3	51
322	Monodisperse Hollow Spheres with Sandwich Heterostructured Shells as High-Performance Catalysts via an Extended SiO2Template Method. Small, 2015, 11, 420-425.	5.2	83
323	Transforming chitosan into N-doped graphitic carbon electrocatalysts. Chemical Communications, 2015, 51, 1334-1337.	2.2	117
324	N-type Cu2O Film for Photocatalytic and Photoelectrocatalytic Processes: Its stability and Inactivation of E. coli. Electrochimica Acta, 2015, 153, 583-593.	2.6	34

#	Article	IF	CITATIONS
325	Photocatalytic and photoelectrocatalytic degradation of small biological compounds at TiO2 photoanode: A case study of nucleotide bases. Catalysis Today, 2015, 242, 363-371.	2.2	17
326	Soil and foliar nutrient and nitrogen isotope composition (\hat{l} 15N) at 5 \hat{A} years after poultry litter and green waste biochar amendment in a macadamia orchard. Environmental Science and Pollution Research, 2015, 22, 3803-3809.	2.7	60
327	Room temperature ferromagnetic Cr–Ni codoped ZnO diluted magnetic semiconductors synthesized by hydrothermal method under high pulsed magnetic field. Ceramics International, 2015, 41, 451-457.	2.3	29
328	Object Classification via Feature Fusion Based Marginalized Kernels. IEEE Geoscience and Remote Sensing Letters, 2015, 12, 8-12.	1.4	31
329	pHâ€Regulated Synthesis of Multiâ€Shelled Manganese Oxide Hollow Microspheres as Supercapacitor Electrodes Using Carbonaceous Microspheres as Templates. Advanced Science, 2014, 1, 1400011.	5 . 6	154
330	Bottom-Up Enhancement of g-C3N4Photocatalytic H2Evolution Utilising Disordering Intermolecular Interactions of Precursor. International Journal of Photoenergy, 2014, 2014, 1-8.	1.4	10
331	Carbonized Nanoscale Metal–Organic Frameworks as High Performance Electrocatalyst for Oxygen Reduction Reaction. ACS Nano, 2014, 8, 12660-12668.	7.3	509
332	Potential for Layered Double Hydroxides-Based, Innovative Drug Delivery Systems. International Journal of Molecular Sciences, 2014, 15, 7409-7428.	1.8	94
333	Synthesis and characterization of N-doped carbonaceous/TiO2 composite photoanodes for visible-light photoelectrocatalytic inactivation of Escherichia coli K-12. Catalysis Today, 2014, 230, 67-73.	2.2	29
334	Core–Shell Palladium Nanoparticle@Metal–Organic Frameworks as Multifunctional Catalysts for Cascade Reactions. Journal of the American Chemical Society, 2014, 136, 1738-1741.	6.6	632
335	Air-processed depleted bulk heterojunction solar cells based on PbS/CdS core–shell quantum dots and TiO2 nanorod arrays. Solar Energy Materials and Solar Cells, 2014, 124, 67-74.	3.0	35
336	Multi-shelled CeO ₂ hollow microspheres as superior photocatalysts for water oxidation. Nanoscale, 2014, 6, 4072-4077.	2.8	262
337	Quintupleâ€Shelled SnO ₂ Hollow Microspheres with Superior Light Scattering for Highâ€Performance Dyeâ€Sensitized Solar Cells. Advanced Materials, 2014, 26, 905-909.	11.1	283
338	Visible-light-driven photocatalytic inactivation of E. coli by Ag/AgX-CNTs (X=Cl, Br, I) plasmonic photocatalysts: Bacterial performance and deactivation mechanism. Applied Catalysis B: Environmental, 2014, 158-159, 301-307.	10.8	149
339	Manipulating solar absorption and electron transport properties of rutile TiO2 photocatalysts via highly n-type F-doping. Journal of Materials Chemistry A, 2014, 2, 3513.	5.2	52
340	UV and visible light photoelectrocatalytic bactericidal performance of 100% {111} faceted rutile TiO2 photoanode. Catalysis Today, 2014, 224, 77-82.	2.2	30
341	Density functional theory analysis of structural and electronic properties of orthorhombic perovskite CH ₃ NH ₃ Pbl ₃ . Physical Chemistry Chemical Physics, 2014, 16, 1424-1429.	1.3	306
342	Novel Environmental Analytical System based on Combined Biodegradation and Photoelectrocatalytic Detection Principles for Rapid Determination of Organic Pollutants in Wastewaters. Environmental Science & Environmental Envi	4.6	22

#	Article	IF	CITATIONS
343	Multishelled TiO ₂ Hollow Microspheres as Anodes with Superior Reversible Capacity for Lithium Ion Batteries. Nano Letters, 2014, 14, 6679-6684.	4.5	406
344	Stable Isolated Metal Atoms as Active Sites for Photocatalytic Hydrogen Evolution. Chemistry - A European Journal, 2014, 20, 2138-2144.	1.7	173
345	Titania single crystals with a curved surface. Nature Communications, 2014, 5, 5355.	5.8	94
346	New Insight into the Role of Gold Nanoparticles in Au@CdS Core–Shell Nanostructures for Hydrogen Evolution. Small, 2014, 10, 4664-4670.	5.2	138
347	Formation Mechanism of Freestanding CH ₃ NH ₃ Pbl ₃ Functional Crystals: In Situ Transformation vs Dissolution–Crystallization. Chemistry of Materials, 2014, 26, 6705-6710.	3.2	143
348	Structure disorder of graphitic carbon nitride induced by liquid-assisted grinding for enhanced photocatalytic conversion. RSC Advances, 2014, 4, 10676-10679.	1.7	28
349	Blue hydrogenated lithium titanate as a high-rate anode material for lithium-ion batteries. Journal of Materials Chemistry A, 2014, 2, 6353.	5.2	58
350	Precisely controlled heterogeneous nucleation sites for TiO ₂ crystal growth. CrystEngComm, 2014, 16, 7502.	1.3	11
351	A {0001} faceted single crystal NiS nanosheet electrocatalyst for dye-sensitised solar cells: sulfur-vacancy induced electrocatalytic activity. Chemical Communications, 2014, 50, 5569.	2.2	60
352	A facile synthesis of single crystal TiO2 nanorods with reactive {100} facets and their enhanced photocatalytic activity. CrystEngComm, 2014, 16, 3091.	1.3	25
353	Directly hydrothermal growth of ultrathin MoS2 nanostructured films as high performance counter electrodes for dye-sensitised solar cells. RSC Advances, 2014, 4, 21277.	1.7	82
354	Reply to the †Comment on †Density functional theory analysis of structural and electronic properties of orthorhombic perovskite CH3NH3PbI3†€ by J. Even et al., Phys. Chem. Chem. Phys., 2014, 10.1039/C3CP55006K. Physical Chemistry Chemical Physics, 2014, 16, 8699-8700.	1.3	2
355	Platinum@regular indium oxide nanooctahedra as difunctional counter electrodes for dye-sensitized solar cells. Journal of Materials Chemistry A, 2014, 2, 6331-6336.	5.2	9
356	Systematic Approach to In-Depth Understanding of Photoelectrocatalytic Bacterial Inactivation Mechanisms by Tracking the Decomposed Building Blocks. Environmental Science & E	4.6	169
357	Highly efficient and recyclable triple-shelled Ag@Fe3O4@SiO2@TiO2 photocatalysts for degradation of organic pollutants and reduction of hexavalent chromium ions. Nanoscale, 2014, 6, 5181.	2.8	115
358	Enhanced photocatalytic activity of hierarchical structure TiO ₂ hollow spheres with reactive (001) facets for the removal of toxic heavy metal Cr(<scp>vi</scp>). RSC Advances, 2014, 4, 34577-34583.	1.7	39
359	Hydrothermal Transformation of Dried Grass into Graphitic Carbonâ€Based High Performance Electrocatalyst for Oxygen Reduction Reaction. Small, 2014, 10, 3371-3378.	5.2	135
360	A self-sponsored doping approach for controllable synthesis of S and N co-doped trimodal-porous structured graphitic carbon electrocatalysts. Energy and Environmental Science, 2014, 7, 3720-3726.	15.6	198

#	Article	IF	Citations
361	One-step synthesis of nitrogen-doped microporous carbon materials as metal-free electrocatalysts for oxygen reduction reaction. Journal of Materials Chemistry A, 2014, 2, 11666-11671.	5.2	84
362	Fluorineâ€Doped Porous Singleâ€Crystal Rutile TiO ₂ Nanorods for Enhancing Photoelectrochemical Water Splitting. Chemistry - A European Journal, 2014, 20, 11439-11444.	1.7	58
363	Microwave-Assisted Fabrication of Nanoparticulate TiO ₂ Microspheres for Synergistic Photocatalytic Removal of Cr(VI) and Methyl Orange. ACS Applied Materials & Samp; Interfaces, 2014, 6, 3008-3015.	4.0	147
364	Determination of lodide via Direct Fluorescence Quenching at Nitrogen-Doped Carbon Quantum Dot Fluorophores. Environmental Science and Technology Letters, $2014, 1, 87-91$.	3.9	74
365	Geometric structure of rutile titanium dioxide (111) surfaces. Physical Review B, 2014, 90, .	1.1	18
366	Anatase TiO2 mesocrystals with exposed (001) surface for enhanced photocatalytic decomposition capability toward gaseous styrene. Catalysis Today, 2014, 224, 216-224.	2.2	38
367	Comparative study on the photoelectrocatalytic inactivation of Escherichia coli K-12 and its mutant Escherichia coli BW25113 using TiO2 nanotubes as a photoanode. Applied Catalysis B: Environmental, 2014, 147, 562-570.	10.8	54
368	Directional synthesis of tin oxide@graphene nanocomposites via a one-step up-scalable wet-mechanochemical route for lithium ion batteries. Journal of Materials Chemistry A, 2014, 2, 10211-10217.	5.2	54
369	Hydrogenation Synthesis of Blue TiO ₂ for High-Performance Lithium-lon Batteries. Journal of Physical Chemistry C, 2014, 118, 8824-8830.	1.5	167
370	Two-dimensional carbon leading to new photoconversion processes. Chemical Society Reviews, 2014, 43, 4281-4299.	18.7	214
371	α-Fe ₂ O ₃ multi-shelled hollow microspheres for lithium ion battery anodes with superior capacity and charge retention. Energy and Environmental Science, 2014, 7, 632-637.	15.6	630
372	Vapor-phase hydrothermal synthesis of rutile TiO2 nanostructured film with exposed pyramid-shaped $(1\ 1\ 1)$ surface and superiorly photoelectrocatalytic performance. Journal of Colloid and Interface Science, 2014, 429, 53-61.	5.0	24
373	Adenovirus inactivation by in situ photocatalytically and photoelectrocatalytically generated halogen viricides. Chemical Engineering Journal, 2014, 253, 538-543.	6.6	20
374	Highly Electrocatalytic Activity of RuO ₂ Nanocrystals for Triiodide Reduction in Dyeâ€Sensitized Solar Cells. Small, 2014, 10, 484-492.	5.2	68
375	Threeâ€Dimensional Graphene/Metal Oxide Nanoparticle Hybrids for Highâ€Performance Capacitive Deionization of Saline Water. Advanced Materials, 2013, 25, 6270-6276.	11.1	499
376	Theoretical Understanding and Prediction of Lithiated Sodium Hexatitanates. ACS Applied Materials & Samp; Interfaces, 2013, 5, 1108-1112.	4.0	10
377	ZnO-doped LiFePO4 cathode material for lithium-ion battery fabricated by hydrothermal method. Materials Chemistry and Physics, 2013, 141, 835-841.	2.0	26
378	A Recyclable Mineral Catalyst for Visible-Light-Driven Photocatalytic Inactivation of Bacteria: Natural Magnetic Sphalerite. Environmental Science & Environmental Science & 11166-11173.	4.6	108

#	Article	IF	Citations
379	A highly crystalline Nb3O7F nanostructured photoelectrode: fabrication and photosensitisation. Journal of Materials Chemistry A, 2013, 1, 6563.	5.2	29
380	Surface hydrogen bonding can enhance photocatalytic H2 evolution efficiency. Journal of Materials Chemistry A, 2013, 1, 14089.	5.2	113
381	Unidirectional suppression of hydrogen oxidation on oxidized platinum clusters. Nature Communications, 2013, 4, 2500.	5.8	197
382	ZnO hollow microspheres with exposed porous nanosheets surface: Structurally enhanced adsorption towards heavy metal ions. Colloids and Surfaces A: Physicochemical and Engineering Aspects, 2013, 422, 199-205.	2.3	86
383	Synthesis and Characterization of Novel Plasmonic Ag/AgX-CNTs (X = Cl, Br, I) Nanocomposite Photocatalysts and Synergetic Degradation of Organic Pollutant under Visible Light. ACS Applied Materials & Degradation of Organic Pollutant under Visible Light. ACS Applied Materials & Degradation of Organic Pollutant under Visible Light. ACS Applied Materials & Degradation of Novel Plasmonic Agrangement (Novel Plasmonic Agrangement Plasmonic Agrangement Plasmonic Agrangement (Novel Plasmonic Agrangement Plasmonic Agrangement Plasmonic Agrangement (Novel Plasmonic Agrangement Plasmonic Agrangement Plasmonic Agrangement Plasmonic Agrangement (Novel Plasmonic Agrangement Plasmonic Agrangement Plasmonic Agrangement Plasmonic Agrangement (Novel Plasmonic Agrangement Plasmonic Agrangement Plasmonic Agrangement Plasmonic Agrangement (Novel Plasmonic Agrangement Plasmonic Agrangement Plasmonic Agrangement Plasmonic Agrangement (Novel Plasmonic Agrangement Plasmonic Agrangement Plasmonic Agrangement Plasmonic Agrangement (Novel Plasmonic Agrangement Plasmonic Agrangement Plasmonic Agrangement Plasmonic Agrangement Plasmonic Agrangement (Novel Plasmonic Agrangement Plasmonic Agrang	4.0	144
384	Comparative study of visible-light-driven photocatalytic inactivation of two different wastewater bacteria by natural sphalerite. Chemical Engineering Journal, 2013, 234, 43-48.	6.6	34
385	One-step fabrication of high performance micro/nanostructured Fe3S4–C magnetic adsorbent with easy recovery and regeneration properties. CrystEngComm, 2013, 15, 2956.	1.3	40
386	Nature of visible-light responsive fluorinated titanium dioxides. Journal of Materials Chemistry A, 2013, 1, 12948.	5.2	26
387	The morphology and optical properties of ZnO crystals fabricated by hydrothermal method under pulsed magnetic field. Physica Status Solidi C: Current Topics in Solid State Physics, 2013, 10, 1276-1279.	0.8	2
388	Active sites on hydrogen evolution photocatalyst. Journal of Materials Chemistry A, 2013, 1, 15258.	5.2	96
389	An environmentally benign LIB fabrication process using a low cost, water soluble and efficient binder. Journal of Materials Chemistry A, 2013, 1, 11543.	5.2	42
390	Photocatalytic and photoelectrocatalytic degradation of small biological compounds: A case study of uridine. Catalysis Today, 2013, 201, 167-174.	2.2	10
391	On the synergistic effect of hydrohalic acids in the shape-controlled synthesis of anatase TiO ₂ single crystals. CrystEngComm, 2013, 15, 3252-3255.	1.3	45
392	Highly efficient overlayer derived from peroxotitanium for dye-sensitized solar cells. Journal of Materials Chemistry A, 2013, 1, 1374-1379.	5.2	18
393	Rutile TiO2 films with 100% exposed pyramid-shaped (111) surface: photoelectron transport properties under UV and visible light irradiation. Journal of Materials Chemistry A, 2013, 1, 2646.	5.2	39
394	{001} facets dominated anatase TiO2: Morphology, formation/etching mechanisms and performance. Science China Chemistry, 2013, 56, 402-417.	4.2	24
395	Titanium dioxide-based DGT for measuring dissolved As(V), $V(V)$, Sb(V), Mo(VI) and W(VI) in water. Talanta, 2013, 105, 80-86.	2.9	72
396	Comparative studies of photocatalytic and photoelectrocatalytic inactivation of E. coli in presence of halides. Applied Catalysis B: Environmental, 2013, 140-141, 225-232.	10.8	37

#	Article	IF	Citations
397	A reagent-free tubular biofilm reactor for on-line determination of biochemical oxygen demand. Biosensors and Bioelectronics, 2013, 45, 213-218.	5.3	20
398	A new insight into regulating high energy facets of rutile TiO2. Journal of Materials Chemistry A, 2013, 1, 4182.	5.2	67
399	Photocatalytic Properties of Graphdiyne and Graphene Modified TiO ₂ : From Theory to Experiment. ACS Nano, 2013, 7, 1504-1512.	7.3	434
400	One dimensional CuInS2–ZnS heterostructured nanomaterials as low-cost and high-performance counter electrodes of dye-sensitized solar cells. Energy and Environmental Science, 2013, 6, 835.	15.6	164
401	Vaporâ€Phase Hydrothermal Growth of Novel Segmentally Configured Nanotubular Crystal Structure. Small, 2013, 9, 3043-3050.	5.2	9
402	Rational screening low-cost counter electrodes for dye-sensitized solar cells. Nature Communications, 2013, 4, 1583.	5.8	365
403	Crossâ€Linked gâ€C ₃ N ₄ /rGO Nanocomposites with Tunable Band Structure and Enhanced Visible Light Photocatalytic Activity. Small, 2013, 9, 3336-3344.	5.2	564
404	Accurate Control of Multishelled Co ₃ O ₄ Hollow Microspheres as Highâ€Performance Anode Materials in Lithiumâ€Ion Batteries. Angewandte Chemie - International Edition, 2013, 52, 6417-6420.	7.2	650
405	Rutile nanowire array electrodes for photoelectrochemical determination of organic compounds. Sensors and Actuators B: Chemical, 2013, 186, 132-139.	4.0	13
406	Accurate Control of Multishelled Co ₃ O ₄ Hollow Microspheres as Highâ€Performance Anode Materials in Lithiumâ€Ion Batteries. Angewandte Chemie, 2013, 125, 6545-6548.	1.6	290
407	Free-standing and bendable carbon nanotubes/TiO2 nanofibres composite electrodes for flexible lithium ion batteries. Electrochimica Acta, 2013, 104, 41-47.	2.6	64
408	Target synthesis of a novel porous aromatic framework and its highly selective separation of CO2/CH4. Chemical Communications, 2013, 49, 2780.	2.2	113
409	Edges of FeO/Pt(111) Interface: A First-Principle Theoretical Study. Journal of Physical Chemistry C, 2013, 117, 1672-1676.	1.5	10
410	Enhanced hydrogen desorption from Mg(BH4)2 by combining nanoconfinement and a Ni catalyst. Journal of Materials Chemistry A, 2013, 1, 3471.	5.2	87
411	Engineering the band gap of bare titanium dioxide materials for visible-light activity: a theoretical prediction. RSC Advances, 2013, 3, 8777.	1.7	31
412	Facet-Dependent Catalytic Activity of Platinum Nanocrystals for Triiodide Reduction in Dye-Sensitized Solar Cells. Scientific Reports, 2013, 3, 1836.	1.6	146
413	Instant inactivation and rapid decomposition of Escherichia coli using a high efficiency TiO2 nanotube array photoelectrode. RSC Advances, 2013, 3, 20824.	1.7	11
414	Bioinspired Synthesis of ZnS Supraparticles toward Photoinduced Dechlorination of $2,2\hat{a}\in^2$, $4,4\hat{a}\in^2$, $5,5\hat{a}\in^2\hat{a}\in$ Hexachlorobiphenyl. Chemistry - an Asian Journal, 2013, 8, 1765-1767.	1.7	13

#	Article	IF	CITATIONS
415	Synthesis and characterization of <scp>TiO₂</scp> nanotube photoanode and its application in photoelectrocatalytic degradation of model environmental pharmaceuticals. Journal of Chemical Technology and Biotechnology, 2013, 88, 1488-1497.	1.6	46
416	Turning Indium Oxide into a Superior Electrocatalyst: Deterministic Heteroatoms. Scientific Reports, 2013, 3, 3109.	1.6	28
417	Photoelectrochemical Properties and Its Application of Nano-TiO2/Boron-doped Diamond Heterojunction Electrode Material. Asian Journal of Chemistry, 2013, 25, 6167-6172.	0.1	12
418	{001} Faceted Anatase Titanium Dioxide Crystals Photoanode for Solar Cells and Photocatalysis. , 2013, , .		0
419	Synthesis and characterization of germanium-centered three-dimensional crystalline porous aromatic framework. Journal of Materials Research, 2012, 27, 1417-1420.	1.2	8
420	Determination of chemical oxygen demand of nitrogenous organic compounds in wastewater using synergetic photoelectrocatalytic oxidation effect at TiO2 nanostructured electrode. Analytica Chimica Acta, 2012, 754, 47-53.	2.6	32
421	Synthesis of Carbon Nanotube–Anatase TiO ₂ Sub-micrometer-sized Sphere Composite Photocatalyst for Synergistic Degradation of Gaseous Styrene. ACS Applied Materials & Interfaces, 2012, 4, 5988-5996.	4.0	128
422	Investigating Arsenic Speciation and Mobilization in Sediments with DGT and DET: A Mesocosm Evaluation of Oxic-Anoxic Transitions. Environmental Science & Evaluation of Oxic-Anoxic Transitions.	4.6	72
423	Low temperature solvothermal synthesis of anatase TiO2 single crystals with wholly $\{100\}$ and $\{001\}$ faceted surfaces. Journal of Materials Chemistry, 2012, 22, 23906.	6.7	91
424	A novel 3D porous cadmium(II) MOF based on conjugated ligand with potential application for sensing small linear conjugated molecule. Inorganic Chemistry Communication, 2012, 25, 74-78.	1.8	17
425	Challenging fabrication of hollow ceramic fiber supported Cu3(BTC)2 membrane for hydrogen separation. Journal of Materials Chemistry, 2012, 22, 10322.	6.7	75
426	Fabrication of mesoporous lignocellulose aerogels from wood via cyclic liquid nitrogen freezing–thawing in ionic liquid solution. Journal of Materials Chemistry, 2012, 22, 13548.	6.7	120
427	Structure, reactivity, photoactivity and stability of Ti–O based materials: a theoretical comparison. Physical Chemistry Chemical Physics, 2012, 14, 2333.	1.3	47
428	Diffusion-Controlled Detection of Trinitrotoluene: Interior Nanoporous Structure and Low Highest Occupied Molecular Orbital Level of Building Blocks Enhance Selectivity and Sensitivity. Journal of the American Chemical Society, 2012, 134, 4978-4982.	6.6	137
429	Vertically aligned nanorod-like rutileTiO2 single crystal nanowire bundles with superior electron transport and photoelectrocatalytic properties. Journal of Materials Chemistry, 2012, 22, 2465-2472.	6.7	84
430	Dehydrogenation of Ammonia Borane Confined by Low-Density Porous Aromatic Framework. Journal of Physical Chemistry C, 2012, 116, 25694-25700.	1.5	30
431	A co-immobilized mediator and microorganism mediated method combined pretreatment by TiO2 nanotubes used for BOD measurement. Talanta, 2012, 93, 314-319.	2.9	15
432	Evaluation of a titanium dioxide-based DGT technique for measuring inorganic uranium species in fresh and marine waters. Talanta, 2012, 97, 550-556.	2.9	36

#	Article	IF	CITATIONS
433	Genetic studies of the role of fatty acid and coenzyme A in photocatalytic inactivation of Escherichia coli. Water Research, 2012, 46, 3951-3957.	5. 3	35
434	High-Performance Nanoporous TiO ₂ /La ₂ O ₃ Hybrid Photoanode for Dye-Sensitized Solar Cells. ACS Applied Materials & Solar Cells.	4.0	62
435	Yolk@shell anatase TiO2 hierarchical microspheres with exposed {001} facets for high-performance dye sensitized solar cells. Journal of Materials Chemistry, 2012, 22, 22082.	6.7	96
436	Synthesis of porous aromatic framework with tuning porosity via ionothermal reaction. Dalton Transactions, 2012, 41, 3933.	1.6	43
437	Vaporâ€Phase Hydrothermal Transformation of HTiOF ₃ Intermediates into {001} Faceted Anatase Singleâ€Crystalline Nanosheets. Small, 2012, 8, 3664-3673.	5.2	56
438	Visible light active pure rutile TiO2 photoanodes with 100% exposed pyramid-shaped (111) surfaces. Nano Research, 2012, 5, 762-769.	5.8	57
439	Nanocrystal Cu2O-loaded TiO2 nanotube array films as high-performance visible-light bactericidal photocatalyst. Applied Microbiology and Biotechnology, 2012, 96, 1201-1207.	1.7	23
440	DGT Measurement of Dissolved Aluminum Species in Waters: Comparing Chelex-100 and Titanium Dioxide-Based Adsorbents. Environmental Science & Environme	4.6	40
441	Single crystal α-Fe2O3 with exposed {104} facets for high performance gas sensor applications. RSC Advances, 2012, 2, 6178.	1.7	82
442	Photocatalytic Synthesis of TiO ₂ and Reduced Graphene Oxide Nanocomposite for Lithium Ion Battery. ACS Applied Materials & Samp; Interfaces, 2012, 4, 3636-3642.	4.0	276
443	Ceria Foam with Atomically Thin Singleâ€Crystal Walls. Angewandte Chemie - International Edition, 2012, 51, 3611-3615.	7.2	18
444	Inorganic Photocatalysts for Overall Water Splitting. Chemistry - an Asian Journal, 2012, 7, 642-657.	1.7	160
445	A New Vaporâ€Phase Hydrothermal Method to Concurrently Grow ZnO Nanotube and Nanorod Array Films on Different Sides of a Zinc Foil Substrate. Chemistry - A European Journal, 2012, 18, 5165-5169.	1.7	20
446	Nano-confined ammonia borane for chemical hydrogen storage. Frontiers of Chemical Science and Engineering, 2012, 6, 27-33.	2.3	37
447	Optimization synthesis of carbon nanotubes-anatase TiO2 composite photocatalyst by response surface methodology for photocatalytic degradation of gaseous styrene. Applied Catalysis B: Environmental, 2012, 123-124, 69-77.	10.8	102
448	A biofilm reactor-based approach for rapid on-line determination of biodegradable organic pollutants. Biosensors and Bioelectronics, 2012, 34, 77-82.	5.3	25
449	Hydrothermal fabrication of rutile TiO2 submicrospheres on wood surface: An efficient method to prepare UV-protective wood. Materials Chemistry and Physics, 2012, 133, 253-258.	2.0	67
450	Nanostructured TiO2 photocatalysts for the determination of organic pollutants. Journal of Hazardous Materials, 2012, 211-212, 381-388.	6.5	33

#	Article	IF	CITATIONS
451	Directly Hydrothermal Growth of Single Crystal Nb ₃ O ₇ (OH) Nanorod Film for High Performance Dyeâ€Sensitized Solar Cells. Advanced Materials, 2012, 24, 1598-1603.	11.1	86
452	A novel low density metal–organic framework with pcu topology by dendritic ligand. Chemical Communications, 2011, 47, 9167.	2.2	63
453	Targeted synthesis of a porous aromatic framework with a high adsorption capacity for organic molecules. Journal of Materials Chemistry, 2011, 21, 13498.	6.7	146
454	A Facile Vapor-Phase Hydrothermal Method for Direct Growth of Titanate Nanotubes on a Titanium Substrate via a Distinctive Nanosheet Roll-Up Mechanism. Journal of the American Chemical Society, 2011, 133, 19032-19035.	6.6	99
455	Naturally Occurring Sphalerite As a Novel Cost-Effective Photocatalyst for Bacterial Disinfection under Visible Light. Environmental Science & Eamp; Technology, 2011, 45, 5689-5695.	4.6	202
456	Structural Transformation, Photocatalytic, and Field-Emission Properties of Ridged TiO ₂ Nanotubes. ACS Applied Materials & Interfaces, 2011, 3, 1352-1358.	4.0	59
457	Lignocellulose Aerogel from Wood-Ionic Liquid Solution (1-Allyl-3-methylimidazolium Chloride) under Freezing and Thawing Conditions. Biomacromolecules, 2011, 12, 1860-1867.	2.6	137
458	Influence of ZnWO4 nanorod aspect ratio on the photocatalytic activity. CrystEngComm, 2011, 13, 4695.	1.3	50
459	Robust TiO2/BDD heterojunction photoanodes for determination of chemical oxygen demand in wastewaters. Analytical Methods, 2011, 3, 2003.	1.3	32
460	Acid degradable ZnO quantum dots as a platform for targeted delivery of an anticancer drug. Journal of Materials Chemistry, 2011, 21, 13406.	6.7	116
461	Anatase TiO ₂ Crystal Facet Growth: Mechanistic Role of Hydrofluoric Acid and Photoelectrocatalytic Activity. ACS Applied Materials & Interfaces, 2011, 3, 2472-2478.	4.0	108
462	Electrodeposition preparation of Ag loaded N-doped TiO2 nanotube arrays with enhanced visible light photocatalytic performance. Catalysis Communications, 2011, 12, 689-693.	1.6	138
463	Rutile nanowire arrays: tunable surface densities, wettability and photochemistry. Journal of Materials Chemistry, 2011, 21, 15806.	6.7	15
464	A selective etching phenomenon on {001} faceted anatase titanium dioxide single crystal surfaces by hydrofluoric acid. Chemical Communications, 2011, 47, 2829.	2.2	124
465	Allelopathic control of cyanobacterial blooms by periphyton biofilms. Environmental Microbiology, 2011, 13, 604-615.	1.8	86
466	Recent applications of TiO2 nanomaterials in chemical sensing in aqueous media. Sensors and Actuators B: Chemical, 2011, 160, 875-890.	4.0	133
467	Controlled synthesis of octahedral Cu2O on TiO2 nanotube arrays by electrochemical deposition. Materials Chemistry and Physics, 2011, 130, 316-322.	2.0	20
468	In situ photoelectrocatalytic generation of bactericide for instant inactivation and rapid decomposition of Gram-negative bacteria. Journal of Catalysis, 2011, 277, 88-94.	3.1	65

#	Article	IF	Citations
469	Electrodeposition of polyhedral Cu2O on TiO2 nanotube arrays for enhancing visible light photocatalytic performance. Electrochemistry Communications, 2011, 13, 861-864.	2.3	120
470	A facile one-step preparation of hierarchically-structured TiO2 nanotube array photoanodes with enhanced photocatalytic activity. Electrochemistry Communications, 2011, 13, 1151-1154.	2.3	11
471	A low cost universal photoelectrochemical detector for organic compounds based on photoelectrocatalytic oxidation at a nanostructured TiO2 photoanode. Journal of Electroanalytical Chemistry, 2011, 656, 211-217.	1.9	15
472	Rutile TiO2 microspheres with exposed nano-acicular single crystals for dye-sensitized solar cells. Nano Research, 2011, 4, 938-947.	5.8	50
473	Layered Fe(III) doped TiO2 thin-film electrodes for the photoelectrocatalytic oxidation of glucose and potassium hydrogen phthalate. Science Bulletin, 2011, 56, 2475-2480.	1.7	3
474	Facile Fabrication of Anatase TiO ₂ Microspheres on Solid Substrates and Surface Crystal Facet Transformation from {001} to {101}. Chemistry - A European Journal, 2011, 17, 5949-5957.	1.7	70
475	Synthesis and characterization of novel SiO2 and TiO2 co-pillared montmorillonite composite for adsorption and photocatalytic degradation of hydrophobic organic pollutants in water. Catalysis Today, 2011, 164, 364-369.	2.2	43
476	Comparing dissolved reactive phosphorus measured by DGT with ferrihydrite and titanium dioxide adsorbents: Anionic interferences, adsorbent capacity and deployment time. Analytica Chimica Acta, 2011, 698, 20-26.	2.6	40
477	Origin of reactivity diversity of lattice oxygen in titanates. Chemical Physics Letters, 2011, 511, 82-86.	1.2	13
478	Electrodeposition preparation of octahedral-Cu2O-loaded TiO2 nanotube arrays for visible light-driven photocatalysis. Scripta Materialia, 2010, 63, 159-161.	2.6	54
479	A Uniquely Configured Acetylcholinesteraseâ€Lecithin Biomimetic Sensing Structure at Cyclohexane/Water Interface for Electrochemical Determination of Fenthion in Organic Solvent. Electroanalysis, 2010, 22, 1061-1065.	1.5	0
480	Environmentally benign periphyton bioreactors for controlling cyanobacterial growth. Bioresource Technology, 2010, 101, 9681-9687.	4.8	50
481	Preparation, characterisation and sensing application of inkjet-printed nanostructured TiO2 photoanode. Sensors and Actuators B: Chemical, 2010, 147, 622-628.	4.0	33
482	A comparative study between photocatalytic and photoelectrocatalytic properties of Pt deposited TiO2 thin films for glucose degradation. Chemical Engineering Journal, 2010, 158, 482-488.	6.6	35
483	The fabrication of CNTs/TiO2photoanodes for sensitive determination of organic compounds. Nanotechnology, 2010, 21, 485503.	1.3	12
484	Fabrication of Highly Ordered TiO ₂ Nanorod/Nanotube Adjacent Arrays for Photoelectrochemical Applications. Langmuir, 2010, 26, 11226-11232.	1.6	62
485	Titanium Dioxide-Based DGT Technique for In Situ Measurement of Dissolved Reactive Phosphorus in Fresh and Marine Waters. Environmental Science & Envi	4.6	97
486	Facile Formation of Branched Titanate Nanotubes to Grow a Three-Dimensional Nanotubular Network Directly on a Solid Substrate. Langmuir, 2010, 26, 1574-1578.	1.6	20

#	Article	IF	CITATIONS
487	Photoelectrochemical Characterization of a Robust TiO ₂ /BDD Heterojunction Electrode for Sensing Application in Aqueous Solutions. Langmuir, 2010, 26, 6033-6040.	1.6	34
488	Anatase TiO2 microspheres with exposed mirror-like plane {001} facets for high performance dye-sensitized solar cells (DSSCs). Chemical Communications, 2010, 46, 8395.	2.2	166
489	Photoelectrochemical quantification of electron transport resistance of TiO2 photoanodes for dye-sensitized solar cells. Physical Chemistry Chemical Physics, 2010, 12, 6625.	1.3	30
490	Direct growth of hierarchically structured titanate nanotube filtration membrane for removal of waterborne pathogens. Journal of Membrane Science, 2009, 343, 212-218.	4.1	23
491	An efficient and low-cost TiO2 compact layer for performance improvement of dye-sensitized solar cells. Electrochimica Acta, 2009, 54, 1319-1324.	2.6	326
492	Degradation of toluene gas at the surface of ZnO/SnO2 photocatalysts in a baffled bed reactor. Research on Chemical Intermediates, 2009, 35, 827-838.	1.3	12
493	A portable miniature UV-LED-based photoelectrochemical system for determination of chemical oxygen demand in wastewater. Sensors and Actuators B: Chemical, 2009, 141, 634-640.	4.0	64
494	In situ photoelectrochemical measurement of phthalic acid on titania. Journal of Photochemistry and Photobiology A: Chemistry, 2009, 208, 97-103.	2.0	6
495	Photoelectrocatalytic activity of mesoporous TiO2 thin film electrodes. Applied Catalysis A: General, 2009, 354, 8-16.	2.2	57
496	A Vapor Phase Hydrothermal Modification Method Converting a Honeycomb Structured Hybrid Film into Photoactive TiO ₂ Film. Langmuir, 2009, 25, 11032-11037.	1.6	48
497	A Portable Photoelectrochemical Probe for Rapid Determination of Chemical Oxygen Demand in Wastewaters. Environmental Science & Environmental Science	4.6	75
498	High-Performance TiO ₂ Photoanode with an Efficient Electron Transport Network for Dye-Sensitized Solar Cells. Journal of Physical Chemistry C, 2009, 113, 16277-16282.	1.5	122
499	Reply to "Comment on Rapid Photoelectrochemical Method for in Situ Determination of Effective Diffusion Coefficient of Organic Compoundsâ€. Journal of Physical Chemistry C, 2009, 113, 10830-10832.	1.5	3
500	Photoelectrocatalytic activity of mesoporous TiO2 films prepared using the sol–gel method with tri-block copolymer as structure directing agent. Journal of Applied Electrochemistry, 2008, 38, 703-712.	1.5	22
501	Photoelectrochemical Manifestation of Photoelectron Transport Properties of Vertically Aligned Nanotubular TiO ₂ Photoanodes. ChemPhysChem, 2008, 9, 117-123.	1.0	39
502	Preparation and characterization of hydrophobic TiO2 pillared clay: The effect of acid hydrolysis catalyst and doped Pt amount on photocatalytic activity. Journal of Colloid and Interface Science, 2008, 320, 501-507.	5.0	63
503	A new geometric biclustering algorithm based on the Hough transform for analysis of large-scale microarray data. Journal of Theoretical Biology, 2008, 251, 264-274.	0.8	51
504	Structural and photocatalytic degradation characteristics of hydrothermally treated mesoporous TiO2. Applied Catalysis A: General, 2008, 350, 237-243.	2,2	81

#	Article	IF	Citations
505	A new approach prevailing over chloride interference in the photoelectrochemical determination of chemical oxygen demand. Analyst, The, 2008, 133, 1684.	1.7	15
506	High-Flux Ceramic Membranes with a Nanomesh of Metal Oxide Nanofibers. Journal of Physical Chemistry B, 2008, 112, 5000-5006.	1.2	49
507	Rapid Photoelectrochemical Method for in Situ Determination of Effective Diffusion Coefficient of Organic Compounds. Journal of Physical Chemistry C, 2008, 112, 3875-3880.	1.5	31
508	Dense TiO _{2 thin film: photoelectrochemical and photocatalytic properties. International Journal of Nanotechnology, 2007, 4, 574.}	0.1	10
509	Photocatalytic Degradation Characteristics of Different Organic Compounds at TiO2Nanoporous Film Electrodes with Mixed Anatase/Rutile Phases. Environmental Science & Environm	4.6	165
510	Novel TiO2 thin film with non-UV activated superwetting and antifogging behaviours. Journal of Materials Chemistry, 2007, 17, 952.	6.7	109
511	Photoelectrocatalytic oxidation of organic compounds at nanoporous TiO2 electrodes in a thin-layer photoelectrochemical cell. Journal of Catalysis, 2007, 250, 102-109.	3.1	62
512	Development of Chemical Oxygen Demand On-Line Monitoring System Based on a Photoelectrochemical Degradation Principle. Environmental Science & Environ	4.6	94
513	Comparison of photocatalytic degradation kinetic characteristics of different organic compounds at anatase TiO2 nanoporous film electrodes. Journal of Photochemistry and Photobiology A: Chemistry, 2006, 177, 253-260.	2.0	41
514	Photoelectrochemical characterisation of TiO2 thin films derived from microwave hydrothermally processed nanocrystalline colloids. Journal of Photochemistry and Photobiology A: Chemistry, 2006, 179, 305-313.	2.0	28
515	Photoelectrocatalytic decontamination of oilfield produced wastewater containing refractory organic pollutants in the presence of high concentration of chloride ions. Journal of Hazardous Materials, 2006, 138, 392-400.	6.5	115
516	Estimation of chemical oxygen demand by ultraviolet spectroscopic profiling and artificial neural networks. Neural Computing and Applications, 2006, 15, 197-203.	3.2	26
517	A rapid analytical method for predicting the oxygen demand of wastewater. Analytical and Bioanalytical Chemistry, 2006, 386, 1773-1779.	1.9	26
518	Metal speciation measurement by diffusive gradients in thin films technique with different binding phases. Analytica Chimica Acta, 2005, 533, 193-202.	2.6	64
519	Oxygen Dependence in a Dual-Phase Electrochemical Biosensing System. Electroanalysis, 2005, 17, 239-245.	1.5	1
520	Ferricyanide-Mediated Microbial Reactions for Environmental Monitoring. ChemInform, 2005, 36, no.	0.1	0
521	Trace metal speciation measurements in waters by the liquid binding phase DGT device. Talanta, 2005, 67, 571-578.	2.9	46
522	Ferricyanide-Mediated Microbial Reactions for Environmental Monitoring. Australian Journal of Chemistry, 2005, 58, 237.	0.5	34

#	Article	IF	Citations
523	Kinetic study of photocatalytic oxidation of adsorbed carboxylic acids at TiO2 porous films by photoelectrolysis. Journal of Catalysis, 2004, 223, 212-220.	3.1	102
524	Photoelectrochemical determination of chemical oxygen demand based on an exhaustive degradation model in a thin-layer cell. Analytica Chimica Acta, 2004, 514, 89-97.	2.6	72
525	Development of a Direct Photoelectrochemical Method for Determination of Chemical Oxygen Demand. Analytical Chemistry, 2004, 76, 155-160.	3.2	170
526	Photoelectrochemical measurement of phthalic acid adsorption on porous TiO2 film electrodes. Journal of Photochemistry and Photobiology A: Chemistry, 2003, 156, 201-206.	2.0	65
527	Characterization of Photoelectrocatalytic Processes at Nanoporous TiO2Film Electrodes:Â Photocatalytic Oxidation of Glucose. Journal of Physical Chemistry B, 2003, 107, 12774-12780.	1.2	118
528	Application of a Poly(4-styrenesulfonate) Liquid Binding Layer for Measurement of Cu2+and Cd2+with the Diffusive Gradients in Thin-Films Technique. Analytical Chemistry, 2003, 75, 2578-2583.	3.2	65
529	Development of a Rapid Ferricyanide-Mediated Assay for Biochemical Oxygen Demand Using a Mixed Microbial Consortium. Analytical Chemistry, 2003, 75, 2584-2590.	3.2	62
530	Synthesis and characterisation of a polyacrylamide–polyacrylic acid copolymer hydrogel for environmental analysis of Cu and Cd. Reactive and Functional Polymers, 2002, 52, 31-41.	2.0	161
531	Preparation and characterisation of a poly(acrylamidoglycolic acid-co-acrylamide) hydrogel for selective binding of Cu2+ and application to diffusive gradients in thin films measurements. Polymer, 2002, 43, 4803-4809.	1.8	66
532	Application of a cellulose phosphate ion exchange membrane as a binding phase in the diffusive gradients in thin films technique for measurement of trace metals. Analytica Chimica Acta, 2002, 464, 331-339.	2.6	54
533	Study on the formation of the Prussian blue films on the polypyrrole surface as a potential mediator system for biosensing applications. Analytica Chimica Acta, 2002, 472, 113-121.	2.6	44
534	The use of microorganisms with broad range substrate utilisation for the ferricyanide-mediated rapid determination of biochemical oxygen demand. Talanta, 2001, 55, 1187-1194.	2.9	56
535	Photoelectrochemical behaviour of methanol oxidation at nanoporous TiO2 film electrodes. Journal of Photochemistry and Photobiology A: Chemistry, 2001, 144, 197-204.	2.0	74
536	A Theoretical Model for Immobilized Enzyme Inhibition Biosensors. Electroanalysis, 2001, 13, 1528-1534.	1.5	21
537	A dual-phase biosensing system for the determination of phenols in both aqueous and organic media. Analytica Chimica Acta, 2001, 441, 95-105.	2.6	26
538	Ferricyanide mediated biochemical oxygen demand–development of a rapid biochemical oxygen demand assay. Analytica Chimica Acta, 2001, 442, 129-139.	2.6	71
539	Development of a quantitative relationship between inhibition percentage and both incubation time and inhibitor concentration for inhibition biosensorsâ€"theoretical and practical considerations. Biosensors and Bioelectronics, 2001, 16, 1119-1126.	5.3	61
540	Development of a fully automated inorganic nitrogen analyzer for continuous, unattended monitoring of water quality. Laboratory Robotics and Automation, 2000, 12, 312-316.	0.3	3

#	Article	IF	Citations
541	Development of a generic microelectrode array biosensing system. Analytica Chimica Acta, 2000, 421, 175-187.	2.6	48
542	Effect of an intermediate on the amperometric response of a polypyrrole-based formate biosensing membrane. Electrochemistry Communications, 2000, 2, 27-31.	2.3	13
543	Conducting electroactive polymer-based biosensors. TrAC - Trends in Analytical Chemistry, 1999, 18, 245-251.	5.8	165
544	Development of an electrochemical flow injection immunoassay (FIIA) for the real-time monitoring of biospecific interactions. Analytica Chimica Acta, 1999, 400, 109-119.	2.6	61
545	Natural Polymer-Based Sulfite Biosensor. Electroanalysis, 1998, 10, 1119-1124.	1.5	40
546	Polypyrrole/poly(2-methoxyaniline-5-sulfonic acid) polymer composite. Polymer Gels and Networks, 1998, 6, 233-245.	0.6	25
547	Synthesis, characterisation and transport properties of layered conducting electroactive polypyrrole membranes. Journal of Membrane Science, 1998, 148, 161-172.	4.1	41
548	Comparative study of electrochemical behaviour of single-crystalline and polycrystalline LaNi5 alloy electrodes. Journal of Alloys and Compounds, 1997, 248, 159-163.	2.8	5
549	Novel conducting polymer-polyelectrolyte composites. Synthetic Metals, 1997, 84, 323-326.	2.1	20
550	Studies of electropolymerisation of sodium 2-(3-thienyl)ethyl sulfonate. Reactive and Functional Polymers, 1997, 34, 27-36.	2.0	1
551	Studies on the performance of Ti2Ni1â^'xAlx hydrogen storage alloy electrodes. Journal of Alloys and Compounds, 1996, 233, 225-230.	2.8	20
552	Effects of yttrium additions on the electrode performance of magnesium-based hydrogen storage alloys. Journal of Alloys and Compounds, 1996, 233, 236-240.	2.8	69
553	Synthesis and electrode characteristics of the new composite alloys Mg2Ni-xwt.% Ti2Ni. Journal of Alloys and Compounds, 1996, 240, 229-234.	2.8	30
554	Detection of cytochrome c using a conducting polymer mediator containing electrode. Electroanalysis, 1996, 8, 248-252.	1.5	13
555	Parameters influencing transport across conducting electroactive polymer membranes. Journal of Membrane Science, 1996, 119, 199-212.	4.1	48
556	Effects of potassium-boron addition on the performance of titanium based hydrogen storage alloy electrodes. International Journal of Hydrogen Energy, 1996, 21, 373-379.	3.8	28
557	On the discharging process of titanium-based hydrogen storage alloy electrode via a.c. impedance analysis. Journal of Power Sources, 1996, 62, 75-79.	4.0	7
558	Pulsed electrochemical detection of proteins using conducting polymer based sensors. Analytica Chimica Acta, 1995, 315, 27-32.	2.6	35

#	Article	IF	CITATIONS
559	Effect of cobalt addition on the performance of titanium-based hydrogen-storage electrodes. Journal of Power Sources, 1995, 55, 197-203.	4.0	39
560	Electrochemically controlled transport in a dual conducting polymer membrane system. Journal of Membrane Science, 1995, 98, 173-176.	4.1	34
561	Mechanism of early capacity loss of Ti2Ni hydrogen-storage alloy electrode. Journal of Power Sources, 1995, 55, 101-106.	4.0	41
562	Characteristics of magnesium-based hydrogen-storage alloy electrodes. Journal of Power Sources, 1995, 55, 263-267.	4.0	69
563	Scratching the Surface of Intelligent Materials: Characterisation Methods for Conducting Polymer Films. Journal of Intelligent Material Systems and Structures, 1994, 5, 605-611.	1.4	4
564	Low-temperature surface micro-encapsulation of Ti2Ni hydrogen-storage alloy powders. Journal of Power Sources, 1994, 52, 295-299.	4.0	27
565	Transport across stand-alone conducting polypyrrole membranes containing dodecylsulfate counterions. Reactive & Functional Polymers, 1994, 23, 213-220.	0.8	25
566	Effect of the counterion employed during synthesis on the properties of polypyrrole membranes. Journal of Membrane Science, 1994, 87, 47-56.	4.1	62
567	Transport of copper(II) across stand-alone conducting polypyrrole membranes: the effect of applied potential waveforms. Polymer, 1993, 34, 16-20.	1.8	37
568	Electrochemically controlled transport of potassium chloride across a conducting electro-active polymer membrane. Journal of Electroanalytical Chemistry, 1992, 334, 111-120.	1.9	59
569	Development of a polymer dispersed-mercury modified electrode. Analytica Chimica Acta, 1990, 238, 345-350.	2.6	20
570	A holistic green system coupling hydrogen production with wastewater valorisation. EcoMat, 0, , .	6.8	1